PHYSICAL REVIEW D **86,** 056005 (2012)

Lepton masses and flavor violation in the Randall-Sundrum model

Abhishek M. Iyer* and Sudhir K. Vempati†

Centre for High Energy Physics, Indian Institute of Science, Bangalore 560012

(Received 16 June 2012; published 18 September 2012)

Lepton masses and mixing angles via localization of 5-dimensional fields in the bulk are revisited in the context of Randall-Sundrum models. The Higgs is assumed to be localized on the IR brane. Three cases for neutrino masses are considered: (a) The higher-dimensional neutrino mass operator (LH.LH), (b) Dirac masses, and (c) Type I seesaw with bulk Majorana mass terms. Neutrino masses and mixing as well as charged lepton masses are fit in the first two cases using χ^2 minimization for the bulk mass parameters, while varying the $\mathcal{O}(1)$ Yukawa couplings between 0.1 and 4. Lepton flavor violation is studied for all the three cases. It is shown that large negative bulk mass parameters are required for the right-handed fields to fit the data in the LH.LH case. This case is characterized by a very large Kaluza-Klein (KK) spectrum and relatively weak flavor-violating constraints at leading order. The zero modes for the charged singlets are composite in this case, and their corresponding effective 4-dimensional Yukawa couplings to the KK modes could be large. For the Dirac case, good fits can be obtained for the bulk mass parameters, c_i, lying between 0 and 1. However, most of the "best-fit regions" are ruled out from flavor-violating constraints. In the bulk Majorana terms case, we have solved the profile equations numerically. We give example points for inverted hierarchy and normal hierarchy of neutrino masses. Lepton flavor violating rates are large for these points. We then discuss various minimal flavor violation schemes for Dirac and bulk Majorana cases. In the Dirac case with minimal-flavor-violation hypothesis, it is possible to simultaneously fit leptonic masses and mixing angles and alleviate lepton flavor violating constraints for KK modes with masses of around 3 TeV. Similar examples are also provided in the Majorana case.

DOI: 10.1103/PhysRevD.86.056005 PACS numbers: 11.25.Wx, 11.30.Hv, 12.15.Ff, 13.35.−r

I. INTRODUCTION

One of the most interesting solutions of the hierarchy problem is the Randall-Sundrum (RS) model [1] which proposes a *warped* extra space dimension compactified on an S_1/Z_2 orbifold. Two branes representing the UV and the IR scales are located at the two end points of the orbifold. In the simplest models, the Standard Model (SM) matter and gauge fields are localized on the IR brane along with the Higgs field. Massive Planck scale modes are exponentially suppressed at the IR brane, due to the warped bulk geometry, caused by the presence of a large negative cosmological constant.[1] Variations of this setup have been considered in several different contexts.[2]

For example, introducing gauge fields in the bulk facilitates unification of couplings [4]. But this leads to large corrections to the electroweak precision observables and places a lower bound on the mass of the lightest-gauge Kaluza-Klein (KK) mode to be around 25 TeV. This is because the coupling of brane-localized fermions to the gauge KK states is enhanced by a factor ~8.5 compared to the SM coupling [5–7]. A similar study in terms of oblique parameters was reported in Refs. [8,9]. Boundary kinetic terms for the gauge fields can lower the bound [10,11], but this might spoil the unification. Alternatively, allowing the fermions to propagate in the bulk eases the constraint of 25 TeV on the lightest KK mode, to about 10 TeV [12]. Having a bulk Higgs further eases the bound [7]. On the other hand, scenarios with extended particle content and a bulk custodial symmetry with a brane-localized Higgs boson were found to lower the bounds on the KK gauge boson mass to ~3 TeV [13]. In Ref. [14], the authors explored a mixed scenario where part of fermions, the third-generation quarks, are localized on the IR brane. It was shown that such a scenario would soften the corrections to the ρ parameter. Finally, modifying the RS metric near the IR boundary can also help in reduction of the strong electroweak precision constraints [15,16].

Allowing fermions to propagate in the bulk has interesting implications for flavor physics. The bulk profiles of the fermion fields are determined by their bulk masses in a manner similar to Arkani-hamed and Schmaltz mechanism in Arkani-Hamed, Dvali, and Dimopolous (ADD) models [17]. In the RS model, however, the warped geometry facilitates the so-called "automatic" localization of fermions [6]. The profiles are also no longer Gaussian, but are exponentially suppressed. It has been proposed that RS could be a theory of flavor, where the fermion mass

*abhishek@cts.iisc.ernet.in
†vempati@cts.iisc.ernet.in

[1]The RS metric is given by

$$ds^2 = e^{-2\sigma(y)}\eta_{\mu\nu}dx^\mu dx^\nu - dy^2,$$

where $\sigma(y) = k|y|$. For recent reviews on RS models, please see Ref. [2].

[2]The phenomenology of RS models has been extensively studied. A recent review on collider phenomenology concentrating on LHC can be found in Ref. [3].

hierarchy can be explained in terms of a few $\mathcal{O}(1)$ parameters. This is analogous to the popular Froggatt-Nielsen (FN) models [18,19] in four dimensions. While in the FN model, it is the gauge and the heavy fermion sector which determine the hierarchies in the Yukawa couplings; in the RS case, it is the geometry of the bulk. The role of the FN charges can be played by the 5-dimensional Dirac masses for the bulk fermions. The expectation is that by taking $\mathcal{O}(1)$ bulk mass parameters as well as Yukawa couplings, one would be able to explain the large hierarchies in the quark and leptonic mass spectrum. While this is true in general for quarks and charged lepton masses, as we will see subsequently, in case of neutrino masses, the situation is a bit more involved.

Flavor violation in the hadronic sector has been explored by various authors [20–22]; a recent comprehensive analysis can be found in Refs. [23,24]. In the present work, we are interested in studying neutrino masses and mixing angles within the RS context. One method of generating neutrino masses in the RS model would be to allow *only* the right-handed neutrino to propagate in the bulk, while the SM particles are confined to the IR brane. This leads to a higher-dimensional seesaw mechanism [25]. However, unlike the case of ADD models, here, only the lightest KK modes participate in the seesaw mechanism. Furthermore, lepton flavor violating decay rates are extremely large in this case pushing the lightest KK mode to be heavier than $m_{\mathrm{kk}} \gtrsim 25$ TeV [26]. Neutrino mass models have also been explored in the alternative scheme where all the fermionic fields are allowed to propagate in the bulk. In the present work, we will concentrate on this setup and study the neutrino mass phenomenology and lepton-flavor violation [25–33]. We have assumed Higgs to be localized on the IR brane. Fermion mass fits in scenarios with Higgs also propagating in the bulk have been considered in RefS. [21,34].

In this RS setup (fermions in the bulk, Higgs localized on IR brane), neutrino mass models can be divided broadly into Dirac mass models or Majorana mass models. In the case of Majorana fermions, the number of possibilities is more than one. In the present work, we discuss three cases in detail: (a) The higher-dimensional LH.LH operator, (b) the Dirac neutrino case, and finally, (c) Majorana neutrinos with bulk seesaw terms. In these models, typically two sets of parameters determine the charged lepton masses and neutrino masses and mixing angles. These are the aforementioned set of bulk Dirac masses for the fermions and then the $\mathcal{O}(1)$ parameters containing the Yukawa couplings. In each of these cases, we have numerically minimized a χ^2 function containing the model parameters and the leptonic masses and mixing data, to determine the best-fit regions of the parameter space. The Yukawa couplings are varied from 0.1 to 4, whereas the ranges for the bulk parameters are judiciously chosen to be as wide as possible.

We found that in the (a) higher-dimensional LH.LH operator case, the bulk mass parameters of the charged singlets are required to be negative and extremely large. This gets reflected into an extremely hierarchal Kaluza-Klein mass spectrum of the first KK states of the SM fermions. In fact, the best-fit regions are those with Standard Model charged singlets being completely composite.[3] On the other hand, if one considers Dirac neutrinos, it is quite possible to fit the data naturally with the bulk Dirac masses within reasonable ranges without any large hierarchies. Both hierarchal and inverse hierarchal neutrino mass schemes can be fit in this case, though it is much more difficult to find regions which satisfy inverse hierarchal neutrino mass relations compared to normal hierarchy. The bulk equations of motion in the presence of a Majorana mass term are coupled and more complicated than the Dirac or LH.LH case. We have solved them numerically and given example points where data can be fit easily either in the inverted or the normal hierarchy scheme. We have not conducted an extended numerical scan of the parameter space for the bulk Majorana case.

Fitting neutrino masses in any of the above models in RS setup potentially leads to large lepton-flavor violation. A detailed analysis was presented in Ref. [30], where the authors discussed the implications of flavor physics in the lepton sector with both the brane localized and the bulk Higgs. Neutrinos were assumed to be of Dirac nature. They observed that with a bulk Higgs, the branching fraction for the process $\mu \to e\gamma$ requires a KK mass scale of around $\sim$20 TeV to keep it below the present experimental limits. Similar comments were made in Ref. [33] on how the higher-dimensional operator case is not conductive for suppressing process like $\mu \to eee$, especially when the KK mass is low. Higgs was allowed to propagate in the bulk in this work. In the present work, we revisited the flavor constraints for all the three cases, concentrating on the best-fit regions in the LH.LH and the Dirac case. For the LH.LH case, the couplings of SM fermions to KK gauge bosons are universal in the best-fit region, leading to no apparent constraint, at least at the leading order from the tree-level flavor-violating decays. However, there are large Yukawa couplings in this model which make it unattractive from perturbation theory point of view. The best-fit region of the Dirac case is strongly constrained from tree-level decays as well as loop-induced decays like $\mu \to e + \gamma$. In the brane localized Higgs scenario we are considering here, the limits from dipole processes are cutoff-dependent. But, for cutoff values close to the first KK mass scale, the limits are comparably much stronger. For the bulk Majorana case, too, the points we have considered display strong constraints from leptonic-flavor violation and are ruled out. One would thus need ways to circumvent these strong limits from lepton-flavor violation.

We explored minimal flavor violation (MFV) ansatz implemented in the RS scenario to evade the flavor

[3]This interpretation is based on the AdS/CFT correspondence.

constraints in the Dirac and Majorana cases [31,35]. We provide example symmetry groups where the flavor-violating constraints can be removed for both the Dirac and the Majorana cases.

The paper is organized as follows. In Sec. II, we discuss lepton mass fits in three models of neutrino mass generation, the higher-dimensional LH.LH operator, the Dirac case, and the bulk Majorana mass terms case spread over three subsections. In Sec. III, we discuss the lepton flavor violating constraints for the three cases of neutrino masses. In Sec. IV, we discuss the minimal-flavor-violating schemes for the Dirac and Majorana cases and show example points where flavor-violating constraints are alleviated. We close with a summary and outlook in the final Sec. V.

II. LEPTON MASS FITS

The observed neutrino and charged lepton data is fit to the set of theory parameters which determine the charged lepton and neutrino mass matrices through a χ^2 minimization. Thus, the observables correspond to three charged lepton masses, three mixing angles, and two (neutrino) mass squared differences, while the bulk mass parameters and Yukawa couplings form the set of theory parameters. The number of theory parameters varies from model to model, as discussed in the following subsections. We have chosen the following central values for the observables [36,37]:

We use the standard χ^2 definition for N observables given by

$$\chi^2 = \sum_{i=1}^{N} \left(\frac{y_i^{\text{exp}} - y_i^{\text{theory}}}{\sigma_i} \right)^2, \tag{1}$$

where, y_i^{theory} is the value of the ith observable predicted by the model and y_i^{exp} is its corresponding experimental number measured with an uncertainty of σ_i. Since the values of the charged lepton are measured to a very high accuracy, it is difficult to fit masses to such high accuracy. Thus, we incorporate up to $\sim$1.5% errors in the masses of charged leptons.[4] The χ^2 relevant to our study is

$$\begin{aligned}\chi^2 = & \frac{(\theta_{\text{sol}} - 0.59)^2}{(0.02)^2} + \frac{(\theta_{\text{atm}} - 0.79)^2}{(0.12)^2} + \frac{(\theta_{13} - 0.154)^2}{(0.02)^2} \\ & + \frac{(\Delta m^2_{\text{sol}} - 7.59 \times 10^{-23})^2}{(0.2 \times 10^{-23})^2} \\ & + \frac{(\Delta m^2_{\text{atm}} - 2.43 \times 10^{-21})^2}{(0.2 \times 10^{-21})^2} + \frac{(m_e - 0.00051)^2}{(0.00001)^2} \\ & + \frac{(m_\mu - 0.1056)^2}{(0.0001)^2} + \frac{(m_\tau - 1.77)^2}{(0.02)^2}. \end{aligned} \tag{2}$$

[4]This approach is very similar to fermion mass fitting in grand unified theories. See, for example, Refs. [38,39].

As mentioned above, the fermion masses (and mass squared differences) and mixing angles appearing in Eq. (2) are functions of bulk parameters. The minimization was performed using MINUIT [40]. For a given scan, MINUIT looks for a local minima for the χ^2 around a certain input guess value of the bulk masses and Yukawa parameters. This scan is repeated by randomly varying the guess values and in the process of looking for a global minima.

A. The LH.LH operator

In the absence of detailed specification of the mechanism which generates neutrino masses, one can always write an effective higher-dimensional operator at the weak scale to account for nonzero neutrino masses. In the Standard Model, this operator is simply the (LH.LH)/Λ operator, where Λ is the high scale at which neutrino masses are generated. In the Randall Sundrum model, one can write a similar operator for nonzero neutrino masses. The model has been earlier studied in Refs. [21,28]. The 5-dimensional action for the RS model with the Higgs localized on the IR brane is given by

$$\begin{aligned} S &= S_{\text{kin}} + S_{\text{Yuk}} \\ S_{\text{kin}} &= \int d^4x \int dy \sqrt{-g} (\bar{L}(i\not{\partial} - m_L)L + \bar{E}(i\not{\partial} - m_E)E) \\ S_{\text{Yuk}} &= \int d^4x \int dy \sqrt{-g} \left(\frac{\kappa}{\Lambda^{(5)}} \text{LHLH} + Y_E \bar{L} E H \right) \delta(y - \pi R), \end{aligned} \tag{3}$$

where $\Lambda^{(5)} \sim 2.2 \times 10^{18}$ GeV is the fundamental 5-dimensional reduced Planck scale and

$$D_M = \partial_M + \Omega_M + \frac{ig_5}{2} \tau^a W_M^a(x, y) + \frac{ig'}{2} Q_Y B_M(x, y) \tag{4}$$

with $\Omega_M = (-k/2e^{-ky} \gamma_\mu \gamma^5, 0)$ being the spin connection, and Q_Y is the hypercharge. M is the 5-dimensional Lorentz index. R is the compactification radius, and κ and Y_E are the coupling of the neutrino mass operator and the Yukawa coupling for the charged leptons, respectively. They are 3-dimensional matrices in flavor space, and we have suppressed the generation indices in writing the above equation. L and E are the 5-dimensional fermionic fields which transform as doublets and singlets, respectively, under the Standard Model $SU(2)_W$ gauge group with the covariant derivative given by Eq. (4) acting accordingly. m_L and m_E are 5-dimensional Dirac masses of the L and E fields. As we will see below, after Kaluza-Klein decomposition, these masses determine the profiles of the zero and higher KK modes in the extra dimension. Since the effective operator is suppressed by the 5-dimensional Planck mass, one can imagine that the neutrino masses are as a result of some fundamental lepton-number violation beyond the 5-dimensional Planck scale.

The left and right components of the L and E fields have different Z_2 properties. These are chosen such that the Z_2-even zero modes correspond to the SM fields. We assign the following Z_2 parity for the $L_{l,r}$ and the $E_{l,r}$ fields, where the subscripts (l, r) correspond to the left- and right-handed components of L and E.[5]

$$Z_2(y)L_l(x,y) \to L_l(x,y), \qquad Z_2(y)L_r(x,y) \to -L_r(x,y)$$
$$Z_2(y)E_r(x,y) \to E_r(x,y), \qquad Z_2(y)E_l(x,y) \to -E_l(x,y),$$

where $Z_2(y)$: $y \to -y$. The 5-dimensional fields can be expanded in terms of the KK modes, with the expansion given by [20,25]

$$\begin{aligned} L_l(x,y) &= \sum_{n=0}^{\infty} \frac{1}{\sqrt{\pi R}} e^{2\sigma(y)} L_l^{(n)}(x) f_L^{(n)}(y); \\ L_r(x,y) &= \sum_{n=0}^{\infty} \frac{1}{\sqrt{\pi R}} e^{2\sigma(y)} L_r^{(n)}(x) \chi_L^{(n)}(y) \\ E_r(x,y) &= \sum_{n=0}^{\infty} \frac{1}{\sqrt{\pi R}} e^{2\sigma(y)} E_r^{(n)}(x) f_E^{(n)}(y); \\ E_l(x,y) &= \sum_{n=0}^{\infty} \frac{1}{\sqrt{\pi R}} e^{2\sigma(y)} E_l^{(n)}(x) \chi_E^{(n)}(y), \end{aligned} \tag{5}$$

where the exponential factor is chosen such that the fields are canonically normalized. The profiles $f_{L,E}$ and $\chi_{L,E}$ are determined by

$$\begin{aligned} (\partial_y + c_L \sigma') f_{L,E}^{(n)}(y) &= m^{(n)} e^{\sigma(y)} \chi_{L,E}^{(n)}(y) \\ (-\partial_y + c_L \sigma') \chi_{L,E}^{(n)}(y) &= m^{(n)} e^{\sigma(y)} f_{L,E}^{(n)}(y), \end{aligned} \tag{6}$$

where the 5-dimensional masses $m_{L,E}$ are written in terms of the fundamental scale as $m_{L,E} = c_{L,E}\sigma'$ and $\sigma' = \partial_y \sigma = k$. The following orthonormality conditions are used for the profiles $f_{L,E}$ and $\chi_{L,E}$ to arrive at Eq. (6):

$$\begin{aligned} &\frac{1}{\sqrt{2\pi R}} \int_{-\pi R}^{\pi R} dy e^{\sigma} \chi_{L,E}^{(n)}(y) \chi_{L,E}^{(m)}(y) \\ &\quad = \frac{1}{\sqrt{2\pi R}} \int_{-\pi R}^{\pi R} dy e^{\sigma} f_{L,E}^{(n)}(y) f_{L,E}^{(m)}(y) = \delta^{nm}, \end{aligned} \tag{7}$$

The above equations decouple for the zero-mode solutions where $m^{(n)} = 0$. The solution for the Z_2-even part, $f_L(y)$ is given as

$$\begin{aligned} f_L^{(0)}(y) &= N_0(c_L) e^{-c_L \sigma' y}; \\ N_0(c_L) &= \sqrt{\pi R} \sqrt{\frac{(1-2c_L)k}{e^{(1-2c_L)k\pi R} - 1}}, \end{aligned} \tag{8}$$

N_0 being the normalization constant. The solution is the same for profile of E, $f_E(y)$, with c_L replaced by c_E. The bulk wave functions are exponentials which peak towards the UV (IR) for $c > 1/2$ ($c < 1/2$) as can be seen from Eq. (8). Typically, particles lighter in mass like leptons require $c > 1/2$, whereas heavier particles like top quark are localized much closer to the IR brane with $c < 1/2$. For the charged leptons and the neutrino masses, one would expect all the corresponding c_i to be $>1/2$. The KK expansions (5) are put into the Yukawa part of the action Eq. (3) leading to

$$S_{\text{Yuk}} = \int d^4x \int_0^{\pi R} dy \frac{1}{\pi R} \sum_{n,m} \left(Y_E \bar{L}^{(n)}(x) f_L^{(n)}(y) E^{(m)}(x) f_E^{(m)}(y) e^{kR\pi} H + \frac{\kappa}{\Lambda^{(5)}} f_L^{(n)}(y) f_L^{(m)}(y) L^{(n)} L^{(m)} H H e^{2kR\pi} \right) \delta(y - \pi R), \tag{9}$$

where we have used $H \to e^{kR\pi} H$ to canonically normalize the Higgs field and suppressed the subscripts (l, r) for the Z_2-even fields. The odd fields are neglected as they are removed from the boundary as a consequence of the Z_2 symmetry. The charged lepton mass matrix and the neutrino mass matrix are determined when the zero modes of the fields are taken. The charged lepton mass matrix, corresponding to the $L^{(0)}E^{(0)}H$ operator in the action, is given by

$$\begin{aligned} \mathcal{M}_e^{(0,0)} &= \frac{v}{\sqrt{2}} \tilde{Y}_E + \mathcal{O}\left(f_L^{(0)}(\pi R) \frac{v^3}{M_{KK}^2} f_E^{(0)}(\pi R) \right) \\ \tilde{Y}_E &= \frac{Y_E}{R\pi} N_0(c_L) N_0(c_E) e^{(1-c_L-c_E)kR\pi}, \end{aligned} \tag{10}$$

where the matrix $\tilde{Y}_E$ can be considered equivalent to the 4-dimensional dimensionless Yukawa couplings. The neutrino mass matrix defined as the coefficient of the $L^{(0)}L^{(0)}HH$ operator in the action is given as

$$\begin{aligned} \mathcal{M}_{\nu_{ij}}^{(0,0)} &= \tilde{\kappa}_{ij} \frac{v^2}{2\Lambda^{(5)}} + \mathcal{O}\left(\frac{1}{M_{\text{KK}}} \left(\frac{f_L^{(0)}(\pi R) v^2}{\Lambda^{(5)}} \right)^2 \right) \\ \tilde{\kappa}_{ij} &= \kappa_{ij} e^{2kR\pi} f_{L_i}(\pi R) f_{L_j}(\pi R) \\ &= \frac{\kappa_{ij}}{R\pi} N_0(c_{L_i}) N_0(c_{L_j}) e^{(2-c_{L_i}-c_{L_j})kR\pi}, \end{aligned} \tag{11}$$

where i, j are generation indices and M_{KK} is the typical mass of higher KK fermions. The corrections are from higher-order KK modes and can be neglected. Before fitting the mass matrices, we introduce new $\mathcal{O}(1)$ Yukawa parameters entering the mass matrices, which are defined as

$$Y_E' = 2kY_E; \qquad \kappa' = 2k\kappa. \tag{12}$$

[5]The γ_5 required to define the left and right components remains the same as in the 4-dimensional case.

TABLE I. Experimental Data

masses (MeV)	mass-squared (eV^2)	mixing angles
$m_e = 0.51^{+0.0000007}_{-0.0000007}$	$\Delta m^2_{12} = 7.59^{+0.20}_{-0.21} \times 10^{-5}$	$\theta_{12} = 0.59^{+0.02}_{-0.015}$
$m_\mu = 105.6^{+0.000003}_{-0.000003}$	$\Delta m^2_{23} = 2.43^{+0.13}_{-0.13} \times 10^{-3}$	$\theta_{23} = 0.79^{+0.12}_{-0.12}$
$m_\tau = 1776^{+0.00016}_{-0.00016}$		$\theta_{13} = 0.154^{+0.016}_{-0.016}$

In terms of these new Yukawa parameters, the mass matrices are explicitly given as

$$(\mathcal{M}_e^{(0,0)})_{ij} = \frac{v}{\sqrt{2}}(Y_E')_{ij} e^{(1-c_L-c_E)k R\pi} \sqrt{\frac{(0.5-c_{L_i})}{e^{(1-2c_{L_i})\pi k R}-1}} \sqrt{\frac{(0.5-c_{E_j})}{e^{(1-2c_{E_j})\pi k R}-1}},$$
$$(\mathcal{M}_\nu^{(0,0)})_{ij} = \frac{v^2}{2\Lambda^{(5)}}(\kappa')_{ij} e^{(2-c_{L_i}-c_{L_j})k R\pi} \sqrt{\frac{(0.5-c_{L_i})}{e^{(1-2c_{L_i})\pi k R}-1}} \sqrt{\frac{(0.5-c_{L_j})}{e^{(1-2c_{L_j})\pi k R}-1}}. \tag{13}$$

The matrices are diagonalized as $U_{eL}^\dagger \mathcal{M}_e^{(0,0)} U_{eR} = \mathrm{Diag}[\{m_e, m_\mu, m_\tau\}]$ and $U_\nu \mathcal{M}_\nu^{(0,0)} U_\nu^T = \mathrm{Diag}[\{m_{\nu_1}, m_{\nu_2}, m_{\nu_3}\}]$ and $U_{\mathrm{PMNS}} = U_\nu^\dagger U_{eL}$. The eigenvalues of the charged lepton mass matrix and the mass-squared differences of the neutrino mass matrix and the U_{PMNS} mixing angles are fit to the data as per Table I. In this case, there are three c_{L_i} and three c_{E_i} and fifteen Yukawa parameters fitting three charged lepton masses, three angles, and two mass squared differences. Given the dependence of the leptonic mass matrices on the Yukawa parameters, we have chosen them strictly to be of $\mathcal{O}(1)$ nature. By this, we mean they are varied roughly between

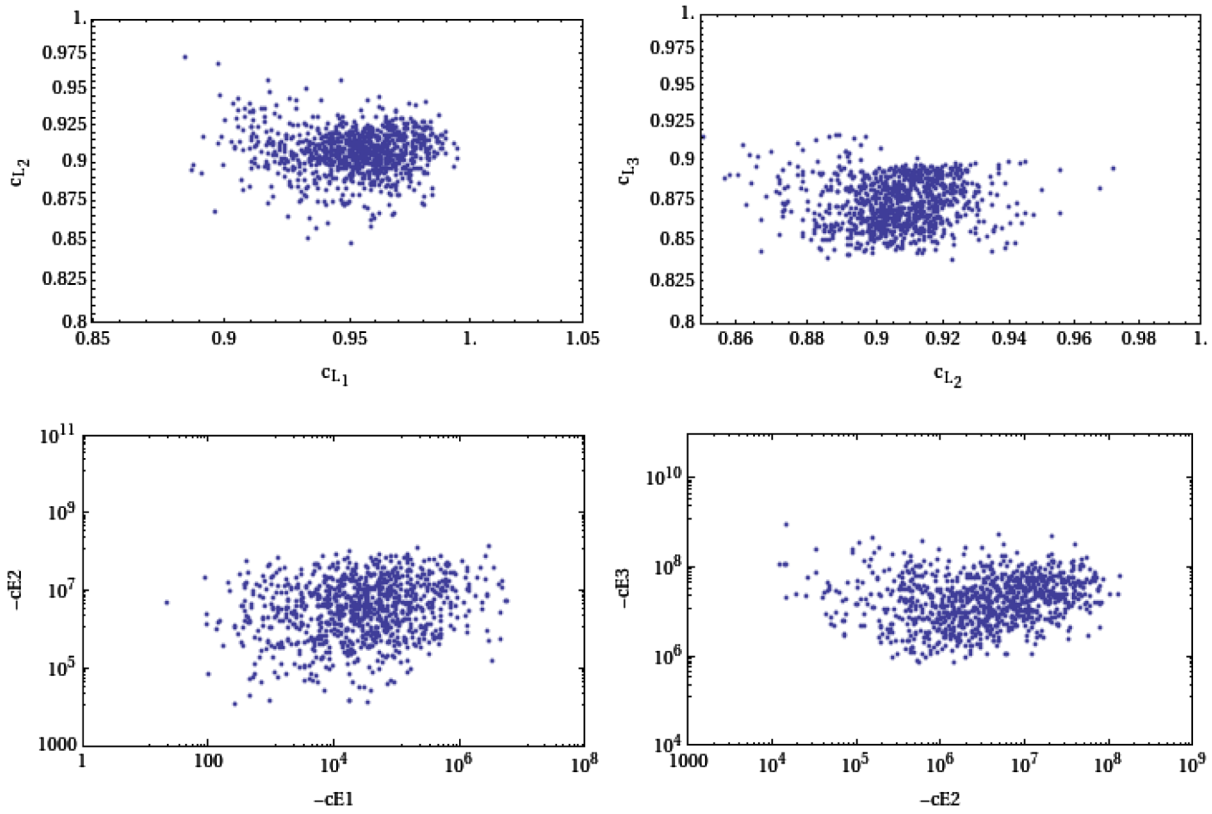

FIG. 1 (color online). Regions in c_i for the LH.LH case which give best fit to lepton masses and mixing. The graphs in the upper row show the region of parameter space for the bulk masses for doublets which fit small neutrino masses. Neutrino masses are assumed to have normal hierarchy in this analysis. The graphs in the lower row show the region for the bulk masses for the charged singlets c_{E_i}. We have used log scale for c_{E_i}

TABLE II. Allowed range for the bulk parameters with minimum χ^2. Neutrino masses have normal hierarchy. Range of first KK scale of the doublet(singlet) $M_L^{(1)}$ ($M_E^{(1)}$) corresponding to the bulk mass parameter is also given.

parameter	range	range of $M_L^{(1)}$ (TeV)	parameter	range	range of $M_E^{(1)}$ (TeV)
c_{L_1}	0.87–0.995	1.49–1.59	c_{E_1}	-10.0 to -5.0×10^6	7.9–3.9×10^6
c_{L_2}	0.86–0.98	1.48–1.58	c_{E_2}	-1.0×10^4 to -1.2×10^8	7.9×10^3–9.5×10^7
c_{L_3}	0.84–0.92	1.47–1.53	c_{E_3}	-7.0×10^5 to -1×10^9	5.5×10^5 7.9×10^8

-4 and 4. Furthermore, in order to avoid regions where the Yukawa parameters are unnaturally close to zero, we put a lower bound on the Yukawas such that $|Y|$ lies between $\sim$0.08 and 4.

Since the charged leptons and neutrinos have relatively light mass spectrum compared to heavy quarks, one would have expected that varying c_L and c_E between $1/2$ and 1 would be sufficient to fit the data. However, in the present context, such values for c_E will not satisfy the data. This is because the neutrino mass matrix depends only on c_{L_i}, and requiring the neutrino masses to be of the $\mathcal{O}(10^{-1})$ eV automatically sets c_{L_i} to be around 0.9, close to the UV brane. The charged lepton mass matrix, which in turn is determined by both c_{L_i} and c_{E_i}, should off-set the effect of c_{L_i} and increase the effective 4-dimensional Yukawa coupling by pushing it toward the IR brane. This can only be achieved by taking large and negative values[6] of the c_{E_i}. The range for the scan of the $c_{L,E}$ has been judiciously chosen between 0.82 and 1.0 for bulk doublets and $-5\times10^7 < c_{E_1} < -0.2$, $-10^8 < c_{E_2} < -8000$, and $-10^9 < c_{E_3} < -9000$ for first-, second-, and third-generation charged singlets, respectively. A larger democratic range does not change the results significantly.

All the parameters, the fifteen Yukawa couplings, and the six $c_{L,E}$ parameters are varied so as to minimize the function in Eq. (2). The points which give a χ^2 between 1 and 8 are considered to give a good fit to the data. In Fig. 1, we present the regions in $c_{L_{1,2,3}}$ and $c_{E_{1,2,3}}$ which have minimum χ^2 assuming normal hierarchy for neutrino masses. It is important to remember that Yukawa couplings are also varied in obtaining this range in the $c_{L,E}$ parameter space. From the figures, we see that the strong constraint of neutrino masses limits the c_{L_i} to be within a limited range. On the other hand, c_E seem to have much larger ranges spanning orders of magnitudes. In particular, c_{E_1} is virtually unconstrained from $\mathcal{O}(-1)$ to $\mathcal{O}(-10^6)$. This is an artifact of the unconstrained lightest neutrino mass, m_{ν_1}. c_{E_2} and c_{E_3} have less freedom as they are constrained by the mass-squared differences. The allowed ranges in the $c_{L,E}$ which satisfy the minimum χ^2 requirement are summarized in Table II.

[6]One way to avoid large negative c parameters would be to consider very large O(1) Yukawa parameters. The required Yukawa couplings are in the range $\sim O(10^3$–$10^4)$ to make any connection with data.

It would be interesting to see distribution of the Yukawa couplings Y_E' and κ' for the best-fit regions of the parameter space. The distributions are presented in Figs. 2 and 3. For most of the Y_E' parameters, there is peaking at the two ends of the range chosen, around 0.2 and 3.8. The exception is the lower 2×2 block of the Yukawa matrix, for which there seems to be a flatter profile for the upper-row parameters $(Y_E')_{22}$ and $(Y_E')_{23}$ and a progressively increasing distribution for the second-row parameters.

For almost all of the Y_E' parameters, peaking seems to be happening at high values $\sim$3.8, except for $(Y_E')_{22}$. There are also second peaks at very low values $\sim$0.2 for some of the parameters. Distributions in κ', on the other hand, show peaks at very large value $\sim$3.8 for the first two generation couplings and very low values $\sim$0.4 for κ'_{33} and κ'_{23}. With the exception of peaks, there is an underlying, though highly subdued, ''anarchical'' nature in the distribution of Y_E' Yukawa couplings.[7] Thus, for a given choice of $\mathcal{O}(1)$ Yukawa couplings within our chosen range (-4 to 4), it seems to be possible to find c values which can fit the data well.[8] From the allowed parameter space, we have randomly chosen two sample points, which we call Point A and Point B, and we provided the corresponding observables in Table III. The corresponding Yukawa couplings are given in Eqs. (14) and (15).

Yukawa coupling matrices for Point A:

$$Y_E' = \begin{bmatrix} 0.5023 & 1.9546 & 3.9730 \\ 3.2482 & 2.9629 & 2.7742 \\ 2.6865 & 2.0383 & 1.2369 \end{bmatrix};$$
$$\kappa' = \begin{bmatrix} 3.8933 & 3.9717 & 3.9818 \\ 3.9717 & -2.6660 & -1.1409 \\ 3.9818 & -1.1409 & 1.4597 \end{bmatrix}. \quad (14)$$

Yukawa coupling matrices for Point B

[7]Anarchy in the Yukawa distributions does not necessarily mean anarchical structure in the mass matrix.

[8]Increasing the scan range for the $\mathcal{O}(1)$ Yukawa couplings from -10 to 10 does not change the gross features of the distributions much. For example, Y_E' are peaked near the end points, showing that the lepton masses in this case prefer large or small Yukawa couplings. The κ' distribution has the same features scaled to 0 to 10 from 0 to 4. The ranges of the $c_{L,E}$ do not change significantly.

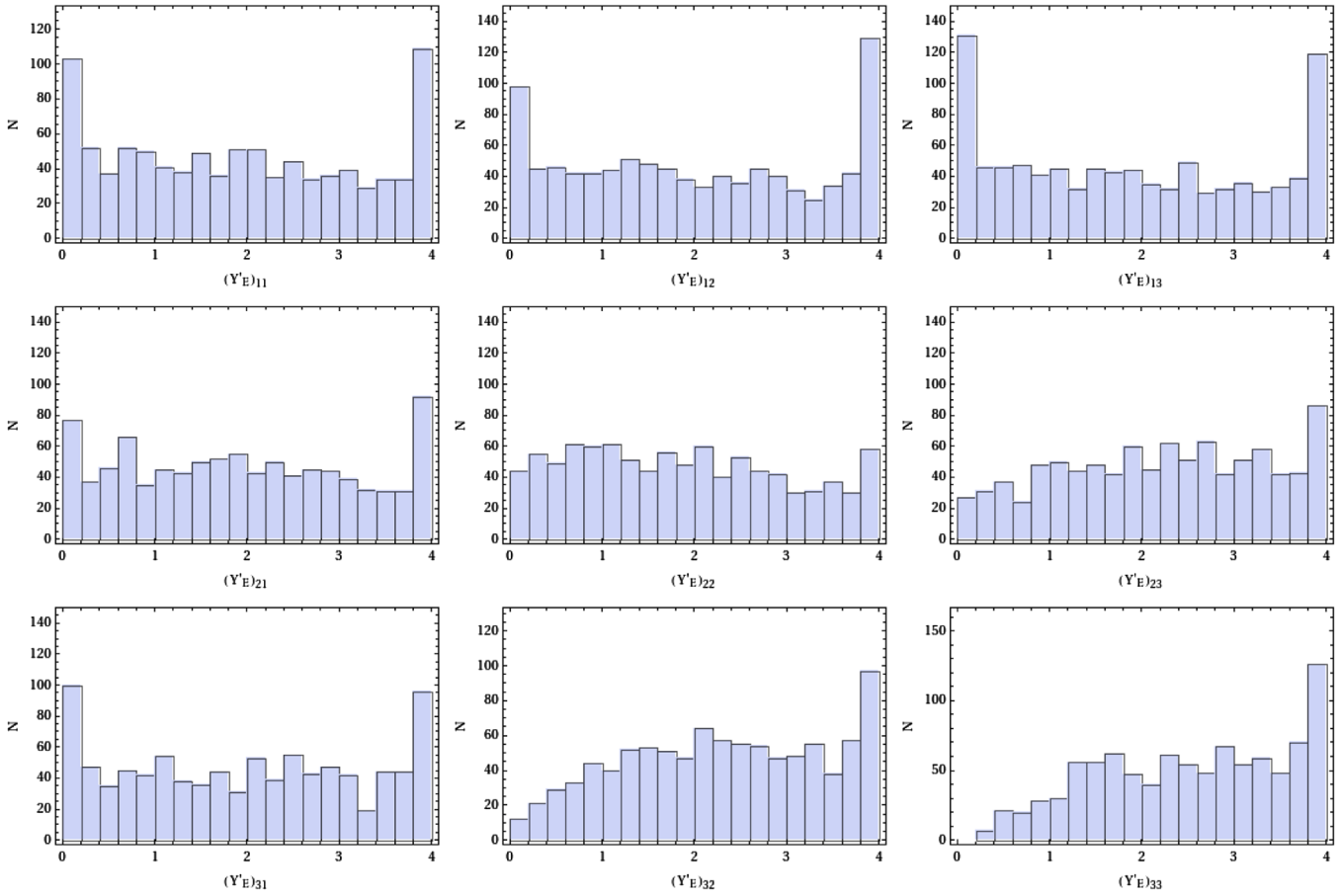

FIG. 2 (color online). The distribution of electron Yukawa couplings (Y'_E) which give a "good fit" to the charged fermion mass data in the LH.LH operator case. Neutrinos are assumed to follow normal hierarchy in this analysis. The binning is done with an interval of 0.2.

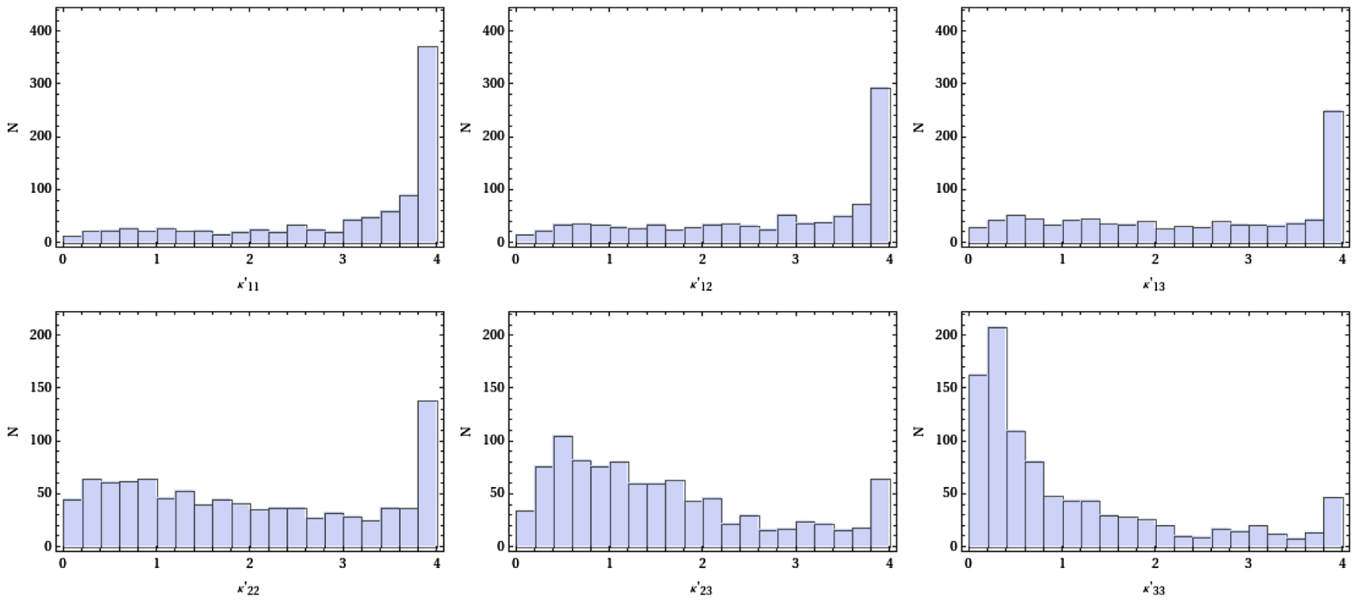

FIG. 3 (color online). The distribution of neutrino Yukawa couplings (κ') which give a good fit to the fermion mass data in the LH.LH operator case. Neutrinos are assumed to follow normal hierarchy in this analysis. The binning is done with an interval of 0.2.

TABLE III. Sample points with corresponding fits of observables for normal hierarchy in LH.LH case with $\mathcal{O}(1)$ Yukawas. The masses are in GeV.

Point	A	B
χ^2	2.07	5.5
c_{L_1}	0.9755	0.903
c_{L_2}	0.9162	0.93
c_{L_3}	0.87	0.8443
c_{E_1}	−692416.99	−17.35
c_{E_2}	−2647794.18	−946125.13
c_{E_3}	−80717122.21	−47941542.53
m_e	5.07×10^{-4}	5.08×10^{-4}
m_μ	0.1056	0.1056
m_τ	1.767	1.771
θ_{12}	0.58	0.589
θ_{23}	0.68	0.743
θ_{13}	.168	0.163
δm^2_{sol}	7.49×10^{-23}	7.48×10^{-23}
δm^2_{atm}	2.47×10^{-21}	1.99×10^{-21}

$$Y'_E = \begin{bmatrix} 3.0571 & 0.6316 & 0.8978 \\ 1.4085 & 0.9952 & 3.5597 \\ 0.7971 & 0.9579 & 0.5539 \end{bmatrix}; \qquad \kappa' = \begin{bmatrix} 0.2315 & -3.8320 & 0.3490 \\ -3.8320 & -0.6632 & -1.1287 \\ 0.3490 & -1.1287 & 0.0802 \end{bmatrix}. \tag{15}$$

In Appendix A, we have presented our results assuming neutrinos have an inverse hierarchical mass ordering. We find very few points which satisfy the data in this case. This is because inverted hierarchical spectrum requires two masses at the atmospheric neutrino scale with their mass difference satisfying Δm^2_{sol}. Thus, the results are very sensitive to the $\mathcal{O}(1)$ Yukawa parameters. For a fixed Yukawa, however, it is easy to find points. More discussion is present in Appendix A.

The analysis presented so far has been purely phenomenological. Let us digress from the fermion fits for a moment to discuss the large negative c parameters. Such large negative values for the bulk mass parameters are in conflict with the 5-dimensional cutoff scale k. We have neglected this conflict in fitting the data where we have considered them to be purely phenomenological parameters which can take any value.[9] In terms of the bulk wave functions, the large negative c values would mean that the zeromode wave function $f^{(0)} \gg 1$, which is not the case when we choose the c parameters between 0 and 1.

[9]We prefer to keep the k (and also the radius R) value fixed by noting that only the charged singlets required large negative c values. In case we shift the 5-dimensional cutoff scale to $|c|k$ keeping k fixed, the corresponding IR would shift to $c\Lambda_{\text{IR}}$, thus spoiling the solution to the hierarchy problem in this scenario.

It is preferable to understand the large negative c values in terms of localization on the IR brane. The limit $c \to -\infty$ corresponds to the case where the fermions are completely localized on the IR singular point [41]. In the limit $c \to -\infty$, $f^{(0)} \to \infty$ indicating full overlap of the bulk wave function with the brane. The value of the c parameters also affects the masses of the KK modes. These masses are determined from Eq. (6) by considering $m_n \neq 0$ and choosing appropriate boundary conditions for the 5-dimensional fields. The resultant differential equation has solution in terms of Bessel's function which describe bulk wave functions of the KK modes, whereas the masses are given in terms of the zeros of the Bessel function [42]. The order of the Bessel function is roughly given by $|c|$ for large values of c. In the asymptotic limit, the first KK mode has mass $\approx |c|ke^{-kR\pi}$. Thus, we see that the phenomenologically relevant first KK mode mass also grows as $\sim c\Lambda_{\text{IR}}$, where $\Lambda_{\text{IR}} \sim$ TeV, the IR cutoff. The masses of the first KK modes are presented in Table II. The bulk wave function of the KK mode tends to zero as $|c| \to \infty$.

One might wonder if such large negative values of the c_{E_i} parameters would have some implications in terms of the AdS/CFT correspondence [2,43]. The conformal field theory interpretation for the bulk scalars has been studied in Refs. [2,44] and for bulk fermions in Ref. [45]. The best-fit $c_{L,E}$ parameters of LH.LH case given in Table II leads to an unusual situation where the left-handed leptons are almost completely elementary while the right-handed singlets are completely composite. This can be easily verified using the "holographic basis" of Ref. [46]. The composite component of the c_L is proportional to $e^{-(c_L-0.5)kR\pi}$, which goes to 0 when $c_L \to 0.99$. Thus, the zero modes for the doublets are elementary. For the c_E fields, however, the elementary component for the zero mode is given as $\sqrt{(c_E-0.5)(c_E+1.5)}e^{-|1.5+c_E|kR\pi}$. Thus, we see that the zero modes for the charged singlets have a vanishing elementary component and thus are dominantly composite fields. The effective 4-dimensional Yukawa coupling of the zero mode to the KK modes is given as $Y'_E\sqrt{(0.5-c_E)}$. A problematic feature of these models is that this coupling enters the nonperturbative regime for c_E large and negative. This nonperturbative coupling appears for all including the first KK mode, which is phenomenologically relevant. This nonperturbative feature is restricted to the Yukawa coupling. The gauge coupling on the other hand does not face this problem. In fact, as we shall see later (Sec. V, Fig. 13), the coupling strength of the zero mode fermions to gauge KK modes quickly approaches the coupling of the brane-localized fermions to gauge bosons for relatively moderate values of $|c|$ parameter.

B. Dirac Neutrinos

Dirac neutrino mass models in the RS setting have been extensively studied in the literature [30]. In Ref. [33], the authors talked about the difficulty of fitting neutrino masses

and mixing angles in the same scenario as quarks. Their argument drew inspiration from the fact that neutrino mixing angles are anarchic in nature. To address this issue, they had a bulk Higgs, with the profile "sufficiently peaked" near the IR brane and introduced a "switching behavior" to fit the charged fermion and the neutrino masses and mixing angles. We, on other hand, approach this problem in the same way as we have done in the LH.LH case of the previous section. We look for regions in the parameter space of the bulk masses which give good fits for a reasonable choice of $\mathcal{O}(1)$ Yukawa couplings. The particle spectrum of the Standard Model is extended by adding singlet right-handed neutrino. Global lepton number is assumed to be conserved. It can be violated by quantum gravity effects which manifest at the 5-dimensional Planck scale. However, for most of the present analysis, we require lepton-number violation present to be highly suppressed.

The bulk and Yukawa actions in Eq. (3) now take the form

$$\begin{aligned} S_{\text{kin}} &= \int d^4x \int dy \sqrt{-g}(\bar{L}(i\not{\partial} - m_L)L + \bar{E}(i\not{\partial} - m_E)E \\ &\quad + \bar{N}(i\not{\partial} - m_N)N) \\ S_{\text{Yuk}} &= \int d^4x \int dy \sqrt{-g}(Y_N \bar{L} N H + Y_E \bar{L} E H)\delta(y - \pi R), \end{aligned} \tag{16}$$

where N stands for the 5-dimensional right-handed neutrino fields. The rest of the parameters carry the same meaning as in the previous section. The components of the N field are assigned the same Z_2 properties as the E field. We expand the N fields as

$$\begin{aligned} N_r(x, y) &= \sum_{n=0}^{\infty} \frac{1}{\sqrt{\pi R}} e^{2\sigma(y)} N_r^{(n)}(x) f_N^{(n)}(y); \\ N_l(x, y) &= \sum_{n=0}^{\infty} \frac{1}{\sqrt{\pi R}} e^{2\sigma(y)} N_l^{(n)}(x) \chi_N^{(n)}(y). \end{aligned} \tag{17}$$

Using Eqs. (17) and (5), one can derive the equations of motion and solutions similar to Eq. (8) for the profiles of N fields. Substituting them, the zero-mode mass matrices for the charged lepton and neutrinos take the form

$$\begin{aligned} \mathcal{M}_e^{(0,0)} &= \frac{v}{\sqrt{2}} \tilde{Y}_E; \\ \tilde{Y}_E &= \frac{Y_E}{R\pi} N_0(c_L) N_0(c_E) e^{(1-c_L-c_E)kR\pi} \\ \mathcal{M}_\nu^{(0,0)} &= \frac{v}{\sqrt{2}} \tilde{Y}_N; \\ \tilde{Y}_N &= \frac{Y_N}{R\pi} N_0(c_L) N_0(c_N) e^{(1-c_L-c_N)kR\pi}, \end{aligned} \tag{18}$$

where we have neglected corrections from higher KK modes. As before, we perform a scan over the parameter space of the bulk fermion masses and order-one Yukawa parameters to minimize the χ^2 in Eq. (2) for the masses and mixing angles. To specify the parameters which are scanned, it is useful to look at the explicit form of the mass matrices equivalent to those of Eq. (13):

$$\begin{aligned} (\mathcal{M}_e^{(0,0)})_{ij} &= \frac{v}{\sqrt{2}} (Y'_E)_{ij} e^{(1-c_{L_i}-c_{E_j})kR\pi} \\ &\quad \times \sqrt{\frac{(0.5 - c_{L_i})}{e^{(1-2c_{L_i})\pi kR} - 1}} \sqrt{\frac{(0.5 - c_{E_j})}{e^{(1-2c_{E_j})\pi kR} - 1}} \\ (\mathcal{M}_\nu^{(0,0)})_{ij} &= \frac{v}{\sqrt{2}} (Y'_N)_{ij} e^{(1-c_{L_i}-c_{N_j})kR\pi} \\ &\quad \times \sqrt{\frac{(0.5 - c_{L_i})}{e^{(1-2c_{L_i})\pi kR} - 1}} \sqrt{\frac{(0.5 - c_{N_j})}{e^{(1-2c_{N_j})\pi kR} - 1}}, \end{aligned} \tag{19}$$

where $Y'_{E,N} = 2kY_{E,N}$. Each of the c_i parameters ($i = \{L, N, E\}$) which are three in number are varied along with eighteen $\mathcal{O}(1)$ Yukawa parameters, i.e., a total of 27 parameters are varied to fit the data and minimize the χ^2. The c parameters are varied as follows: The doublets (c_{L_i}) and the charged singlets are varied between 0.02 and 1,

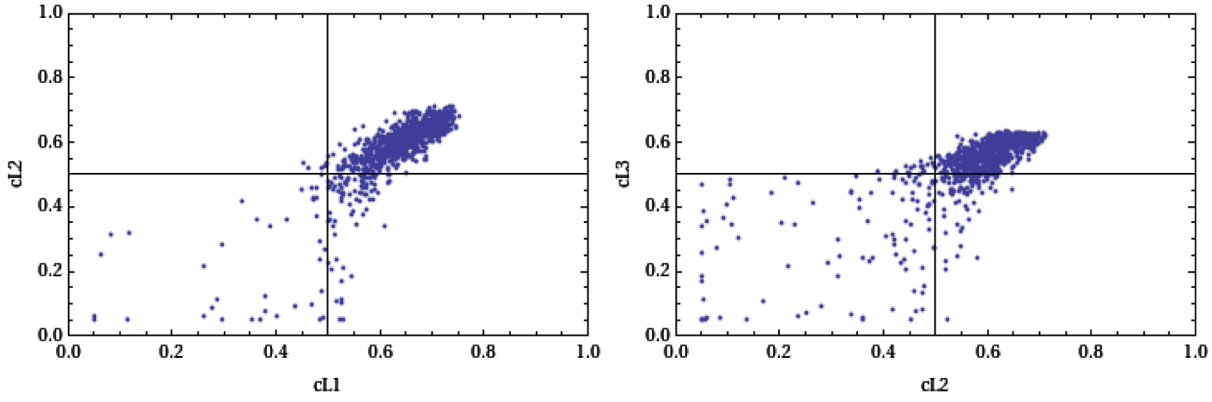

FIG. 4 (color online). The figures above correspond to the case in which neutrinos are of Dirac type. The points in the above figures correspond to a χ^2 between 1 and 8. The plot represents the parameter space for the bulk masses of the doublets. This case corresponds to the normal hierarchial case.

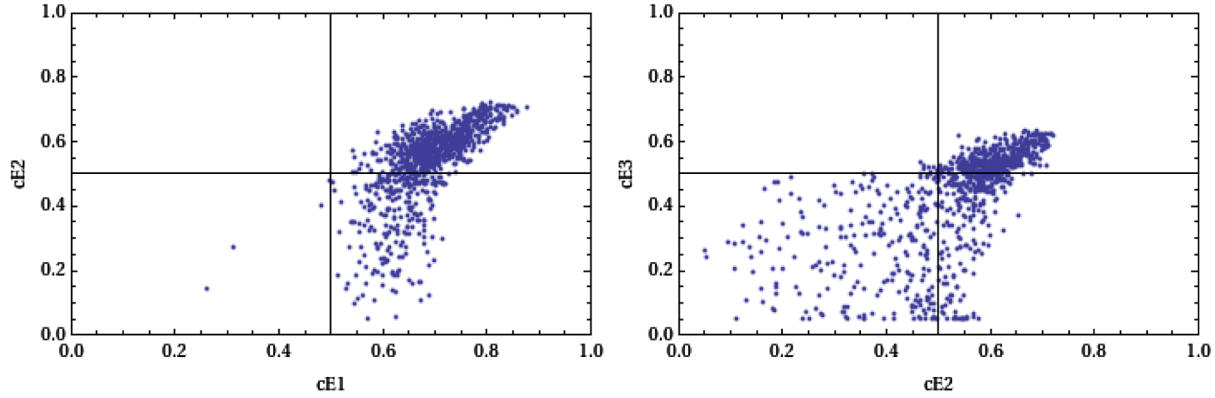

FIG. 5 (color online). The plot represents the parameter space for the bulk masses of charged singlets.

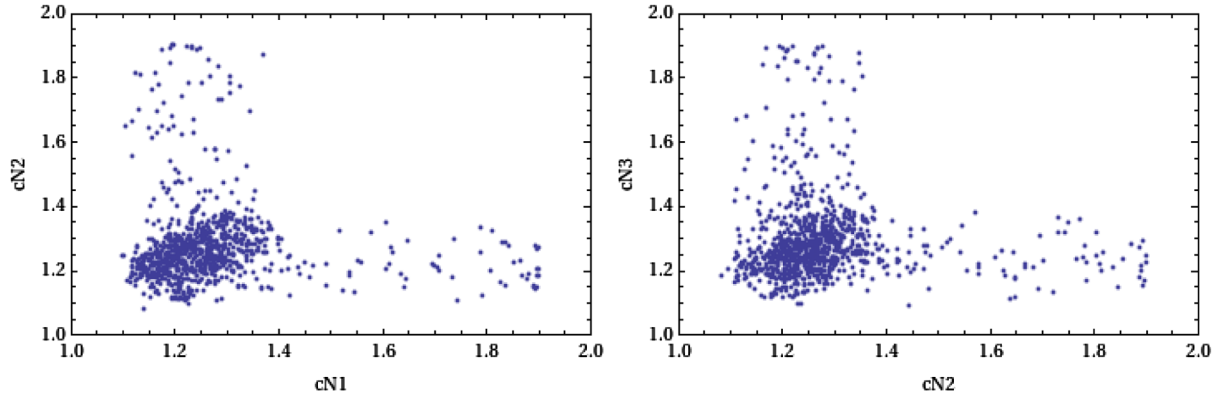

FIG. 6 (color online). The plot represents the parameter space for the bulk masses of the neutrino singlets.

while the neutral singlets are varied between 1 and 1.9. The order-one Yukawa couplings, $Y'_{E,N}$, are varied randomly between -4 and 4 with a lower bound $|Y| \gtrsim 0.08$. We consider all the regions of the c_i parameter space where the χ^2 is between 1 and 8 as a good-fit region. In Figs. 4–6, we present regions in the c_i parameter space which give good fit to the leptonic mass and mixing angles. A summary of these regions is presented in Table IV.

The Dirac neutrino mass matrix in the RS model seems to fit the data more naturally compared to the LHLH discussed in the previous subsection. A large section of the points fall in the regime $c_i > 1/2$ indicating that they are localized closer to the UV brane. The distributions of the Yukawa couplings in the good-fit region, presented in Figs. 7 and 8 show that most of them peak in the last bins for all the Yukawas at (3.8–4.0). A secondary peak can also been seen at the (0.2–0.4) bin for some of the Y'_N parameters. Electron Yukawa couplings on the other hand do not seem to show any such secondary peak. In this case, too, the distribution of the $\mathcal{O}(1)$ Yukawa couplings displays an underlying anarchic nature, especially for the Y'_E. This will prove useful in our analysis of minimal flavor violation where the $\mathcal{O}(1)$ Yukawa couplings and the bulk mass matrices need to be simultaneously diagonalizable. In Table V, we presented two sample points. Point A has all the $c_i > 1/2$, whereas Point B has c_{E_2}, $c_{E_3} < 1/2$. The corresponding Yukawa couplings are given in Eqs. (20) and (21).

As before, we use the holographic basis to comment on the partial compositeness of the bulk fermions. The zero

TABLE IV. Allowed ranges of bulk parameters with normal hierarchy of neutrino masses. The range of first KK scale corresponding to the range of c values is also given.

parameter	range	$M_L^{(1)}$ TeV	parameter	range	$M_E^{(1)}$ TeV	parameter	range	$M_\nu^{(1)}$ TeV
c_{L_1}	0.05–0.76	0.839–1.4	c_{E_1}	0.2–0.88	0.959–1.5	c_{N_1}	1.1–1.9	1.67–2.31
c_{L_2}	0.05–0.72	0.839–1.37	c_{E_2}	0.05–0.73	0.839–1.38	c_{N_2}	1.1–1.9	1.67–2.31
c_{L_3}	0.05–0.64	0.839–1.31	c_{E_3}	0.05–0.64	0.839–1.31	c_{N_3}	1.1–1.9	1.67–2.31

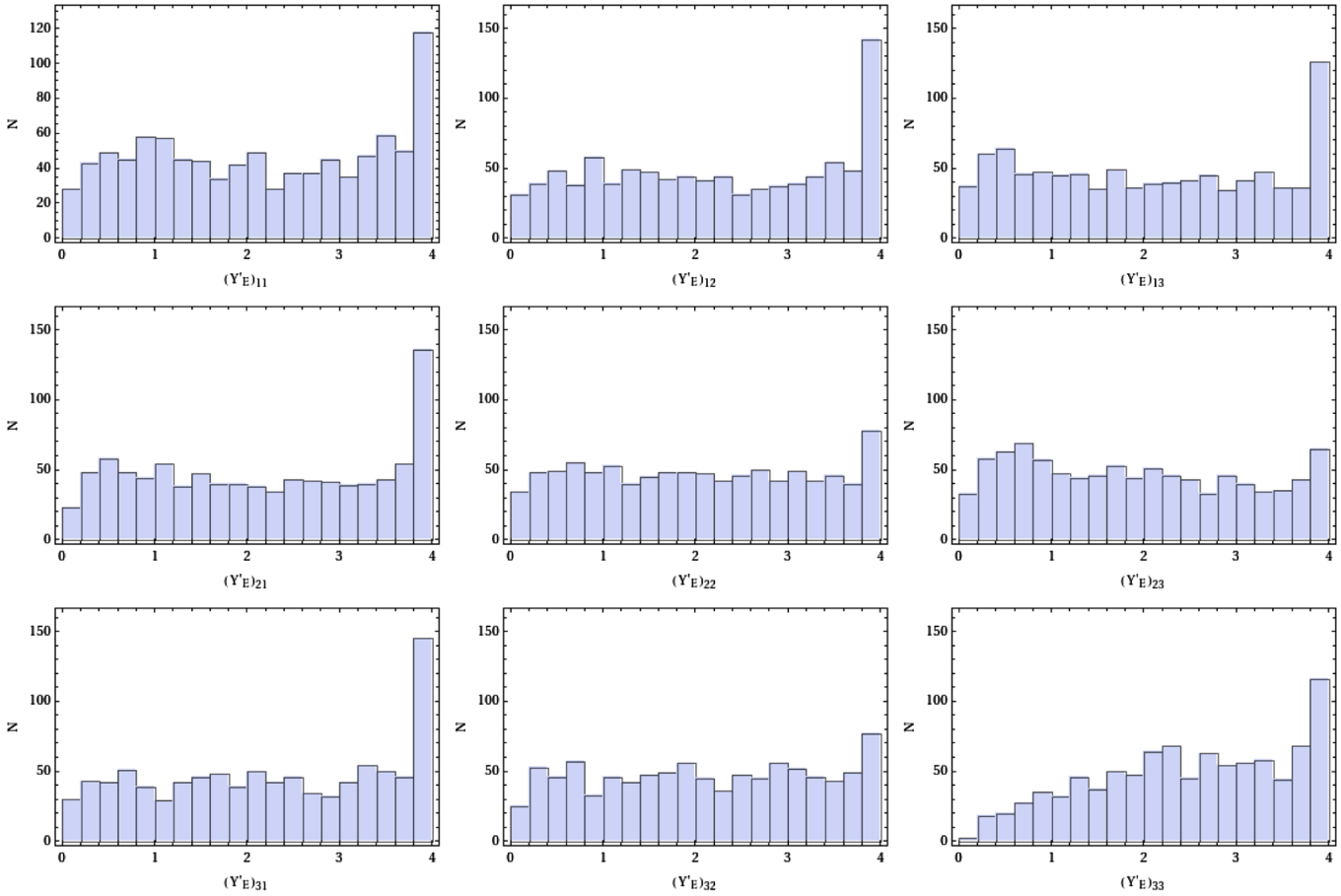

FIG. 7 (color online). The distribution of electron Yukawa couplings (Y'_E) which give a good fit to the fermion mass data in the Dirac case. Neutrinos are assumed to follow normal hierarchy in this analysis. The binning is done with an interval of 0.2.

modes of singlet right-handed neutrinos are dominantly elementary, with an almost zero component of compositeness. The composite component for the zero modes of the doublets and the charged singlets becomes smaller as the corresponding c values become greater than 0.5. Essentially, they have partially composite nature.

Yukawa Coupling Matrix for Point A:

$$Y'_E = \begin{bmatrix} 3.9502 & -1.6538 & 0.5889 \\ -0.7276 & -2.0054 & -3.9004 \\ -1.4061 & 1.4756 & 1.5318 \end{bmatrix};$$
$$Y'_N = \begin{bmatrix} -3.8918 & -3.9447 & -3.8380 \\ -2.6439 & 2.5796 & 3.9962 \\ -0.9223 & -1.3577 & 0.6417 \end{bmatrix}. \quad (20)$$

Yukawa Coupling Matrix for Point B:

$$Y'_E = \begin{bmatrix} 3.3847 & 1.8639 & -1.3814 \\ -1.8107 & -0.7219 & -0.9499 \\ -2.5435 & -1.0497 & -3.3588 \end{bmatrix};$$
$$Y'_N = \begin{bmatrix} 2.4435 & -1.8006 & -1.9575 \\ 0.4198 & -3.1594 & 3.5905 \\ -0.2505 & 1.3172 & 2.1521 \end{bmatrix}. \quad (21)$$

C. Bulk Majorana mass term

Singlet neutrinos typically accommodate Majorana mass terms in addition to the Dirac mass terms. These bare mass terms which break lepton number at a very high scale play an essential role in the standard 4-dimensional seesaw mechanism to generate light neutrino masses. The seesaw mechanism with bulk Majorana mass terms has been first considered in Ref. [29]. There have been other works which have considered brane-localized Majorana mass terms [35,41,47,48]. Our analysis follows the work of Ref. [29] and extends it by computing the numerical solutions. The part of the action which contains the singlet right-handed neutrinos is given by

$$S_N = \int d^4x \int dy \sqrt{-g} (m_M \bar{N} N^c + m_D \bar{N} N + \delta(y - \pi R) Y_N \bar{L} \tilde{H} N), \quad (22)$$

where $N^c = C_5 \bar{N}^T$ with C_5 being the 5-dimensional charge conjugation matrix[10] and $m_M = c_M k$, with k being the

[10] C_5 is taken to be C_4.

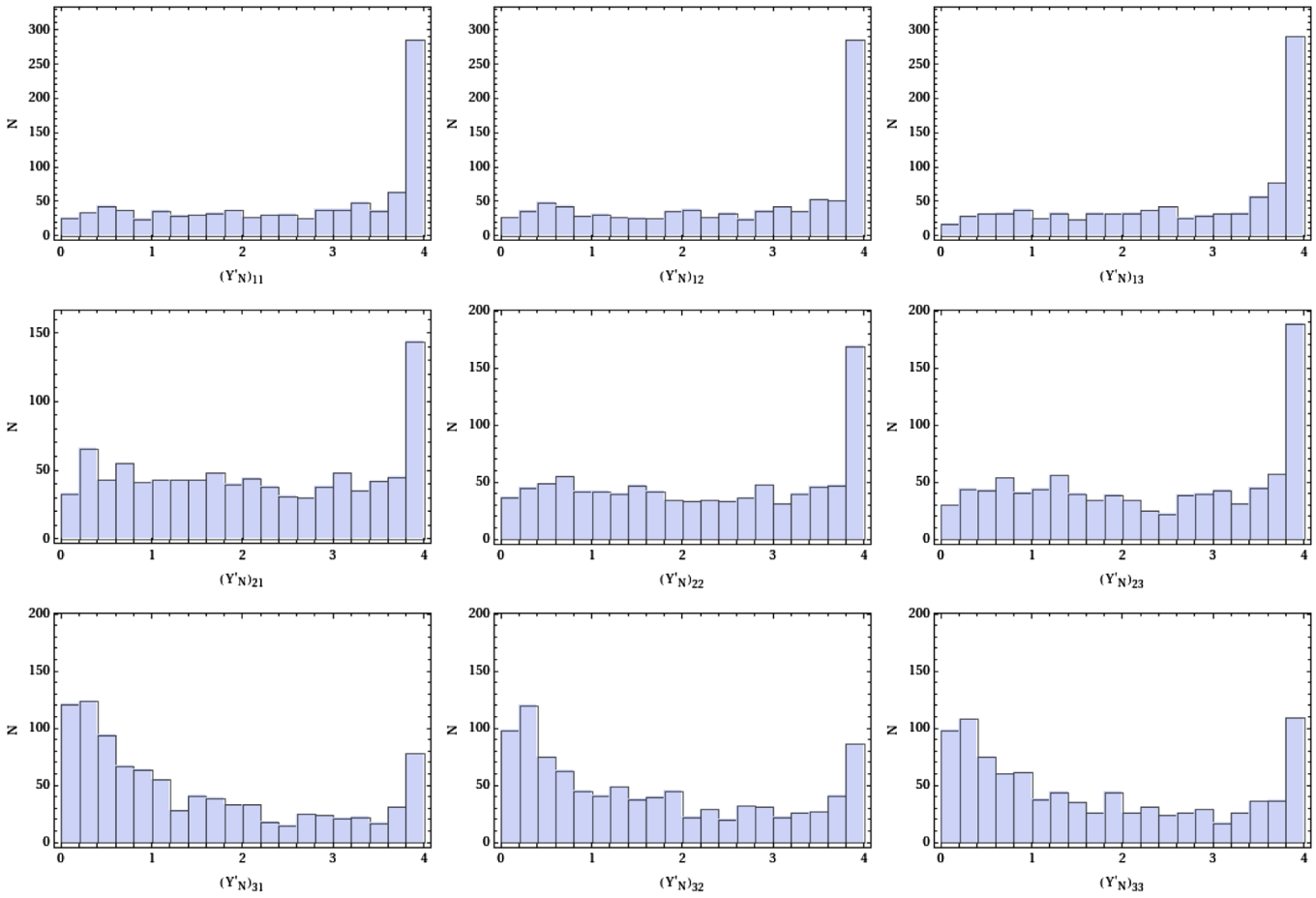

FIG. 8 (color online). The distribution of neutrino Yukawa couplings (Y'_N) which give a good fit to the fermion mass data in the Dirac case. Neutrinos are assumed to follow normal hierarchy in this analysis. The binning is done with an interval of 0.2.

reduced Planck scale.[11] The bulk Dirac mass for the right-handed neutrino is parametrized as $m_D = c_N k$. As before, we consider all the mass parameters to be real. The bulk singlet fields N have the following KK expansions:

$$N_L(x,y) = \sum_{n=0}^{\infty} \frac{1}{\sqrt{\pi R}} e^{2\sigma(y)} N_L^{(n)}(x) g_L^{(n)}(y);$$
$$N_R(x,y) = \sum_{n=0}^{\infty} \frac{1}{\sqrt{\pi R}} e^{2\sigma(y)} N_R^{(n)}(x) g_R^{(n)}(y), \quad (23)$$

where g_L and g_R are profiles of the singlet neutrinos in the bulk. They follow the following orthonormal conditions:

$$\frac{1}{2\pi R} \int_{-\pi R}^{\pi R} dy e^{\sigma} (g_L^{(n)} g_L^{(m)} + g_R^{(n)} g_R^{(m)}) = \delta^{(n,m)}. \quad (24)$$

Using this, the eigenvalues equations for the $g_{L,R}$ fields become [29]

[11] Majorana mass terms do not have the same interpretation in the bulk as in 4 dimensions.

TABLE V. Sample points with corresponding fits of observables for normal hierarchy in the Dirac case with O(1) Yukawas. The masses are in GeV.

Parameter	Point A	Point B
χ^2	0.28	0.39
c_{L_1}	0.6263	0.7166
c_{L_2}	0.5932	0.6382
c_{L_3}	0.5293	0.6126
c_{E_1}	0.6704	0.5911
c_{E_2}	0.5541	0.1939
c_{E_3}	0.5131	0.2647
c_{N_1}	1.2233	1.2791
c_{N_2}	1.2692	1.1215
c_{N_3}	1.2948	1.2343
m_e	5.09×10^{-4}	5.09×10^{-4}
m_μ	0.1055	0.1055
m_τ	1.77	1.77
θ_{12}	0.59	0.589
θ_{23}	0.80	0.792
θ_{13}	0.153	0.153
δm^2_{sol}	7.49×10^{-23}	7.49×10^{-23}
δm^2_{atm}	2.39×10^{-21}	2.40×10^{-21}

$$(\partial_y + m_D) g_L^{(n)}(y) = m_n e^{\sigma} g_R^{(n)}(y) - m_M g_R^{(n)}(y)$$
$$(-\partial_y + m_D) g_R^{(n)}(y) = m_n e^{\sigma} g_L^{(n)}(y) - m_M g_L^{(n)}(y), \quad (25)$$

where we have assumed the 5-dimensional wave functions to be real. Unlike the Dirac and higher-dimensional LHLH term cases, the present system of equations, in Eq. (25), are not consistent with a zero-mode solution $m_n = 0$ for $m_D \neq 0$. This is because the zero-mode solutions, $\propto e^{\sqrt{c_N^2 - c_M^2}\sigma}$ do not satisfy either Dirichlet or the more general $(\partial_y + m_d) g_L(y) = 0$ boundary condition. Thus, in the following analysis, we will consider the first KK mode not to be the zero mode but $m_n = m_{(1)}$. Furthermore, Eq. (25) does not have simple analytical solutions, though numerical solutions exist. We have obtained the numerical solutions of $g_{L,R}$ by solving the second-order equations derived from Eq. (25). The equation for the Z_2-even part takes the form

$$g_L''(y) - \frac{m_n k R e^{kRy}}{m_n e^{kRy} - c_M k} g_L'(y) - \left(\frac{c_N m_n e^{kRy} k^2}{m_n e^{kRy} - c_M k} + c_N^2 k^2 - (m_n e^{kRy} - c_M k)^2 \right) R^2 g_L(y) = 0. \quad (26)$$

The second-order equation for the Z_2-odd part g_R is given as

$$g_R''(y) - \frac{m_n k R e^{kRy}}{m_n e^{kRy} - c_M k} g_R'(y) - \left(\frac{-c_N m_n e^{kRy} k^2}{m_n e^{kRy} - c_M k} + c_N^2 k^2 - (m_n e^{kRy} - c_M k)^2 \right) R^2 g_R(y) = 0, \quad (27)$$

where we have used the notation $m_D = c_N k$ and $M_M = c_M k$ introduced earlier. The primes on $g_L(y)$ and $g_R(y)$ indicate derivatives on the profiles. For a given choice of c_N and c_M, one would expect to numerically find solutions using the above equations for $g_{L,R}$ as long as they satisfy two conditions: (i) $m_{(1)}$ is also fixed such that the boundary conditions are satisfied consistently; (ii) there are no singularities in coefficients of the differential equations in the interval $[0, \pi R]$. This second condition requires that for unique solutions, only those values of c_M and m_n are allowed for which $m_n e^{\sigma} - m_M$ is nonzero. Note that this condition is always true when c_M is negative. For positive c_M, the allowed region is shown in Fig. 9, where all the shaded region has $m_n e^{\sigma} - m_M$ nonzero. As can be seen from the figure, as c_M increases, the KK mass scale also increases. In Fig. 10, we show solutions to Eq. (26) for a fixed value of $c_N = 0.58$. c_M is varied from 0.55 to 1. From the figure, it is clear that the profile becomes oscillatory as

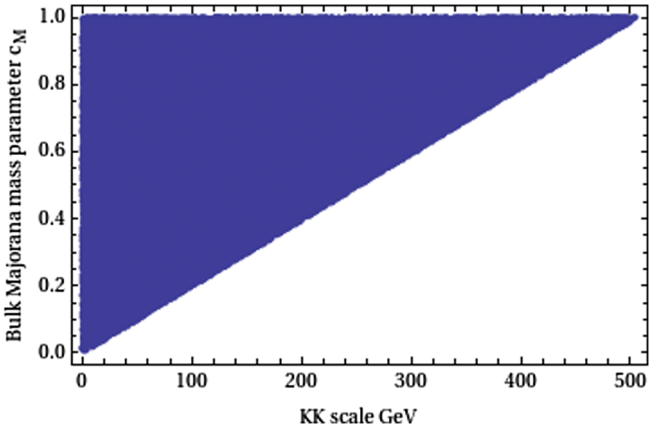

FIG. 9 (color online). Region of c_M-m_1 parameter space, for positive c_M for which the coefficients of the differential equation in Eq. (26) are analytic in the interval $[0, \pi R]$.

c_M becomes greater than c_N. In fact, the solutions are sinusoidal for $c_M = 1$ and $c_N = 0$. We now address the question of fitting the lepton masses and mixing. The charged lepton mass matrix has the same form as in earlier sections:

$$m_l^{(0,0)} = \frac{v}{\sqrt{2}} \tilde{Y}_E + O\left(\frac{v^2}{M_{KK}^2}\right); \quad (28)$$
$$\tilde{Y}_E = \frac{Y_E}{R\pi} N_0(c_L) N_0(c_E) e^{(1-c_L-c_E)kR\pi}.$$

Choosing $g_L^{(1)}$ to be the Z_2-even profile for the right-handed neutrino, the Dirac mass matrix takes the form

$$m_D^{(0,1)} = \frac{Y_N}{R\pi} N_0(c_L) e^{(1-c_L)kR\pi} g_L^{(1)}(\pi R), \quad (29)$$

where $g_L^{(1)}(y)$ is the solution to Eq. (26). The singlet Majorana mass matrix is determined in the flavor space by the choice of c_N and c_M for each of the generations. For simplicity, for the present analysis, we take all of them equal $c_{N_i} = c_N$ and $c_{M_i} = c_M$ for all the three generations.[12] With this, singlet neutrino mass matrix becomes proportional to the unit matrix $M_R = \mathbf{1} m_{(1)}$. The light neutrino mass matrix now takes the seesaw form given by

$$m_\nu^{(0,0)} = m_D^{(0,1)} \frac{1}{M_R} m_D^{(0,1)T} + \mathcal{O}\left(\frac{(m_D^{(0,k)})^2}{m_{(k)}}\right), \quad (30)$$

where higher-order corrections are from higher KK states. To fit the neutrino masses and mixing angles, we neglect higher-order corrections as before. Defining $Y_N' = 2kY_N$, we have

$$m_\nu^{(0,0)} = Y_N' e^{(1-c_L)kR\pi} g_L(\pi R) (M_R^{-1}) Y_N' e^{(1-c_L)kR\pi} g_L(\pi R). \quad (31)$$

[12]This can be achieved by imposing an $O(3)$ symmetry on the N fields.

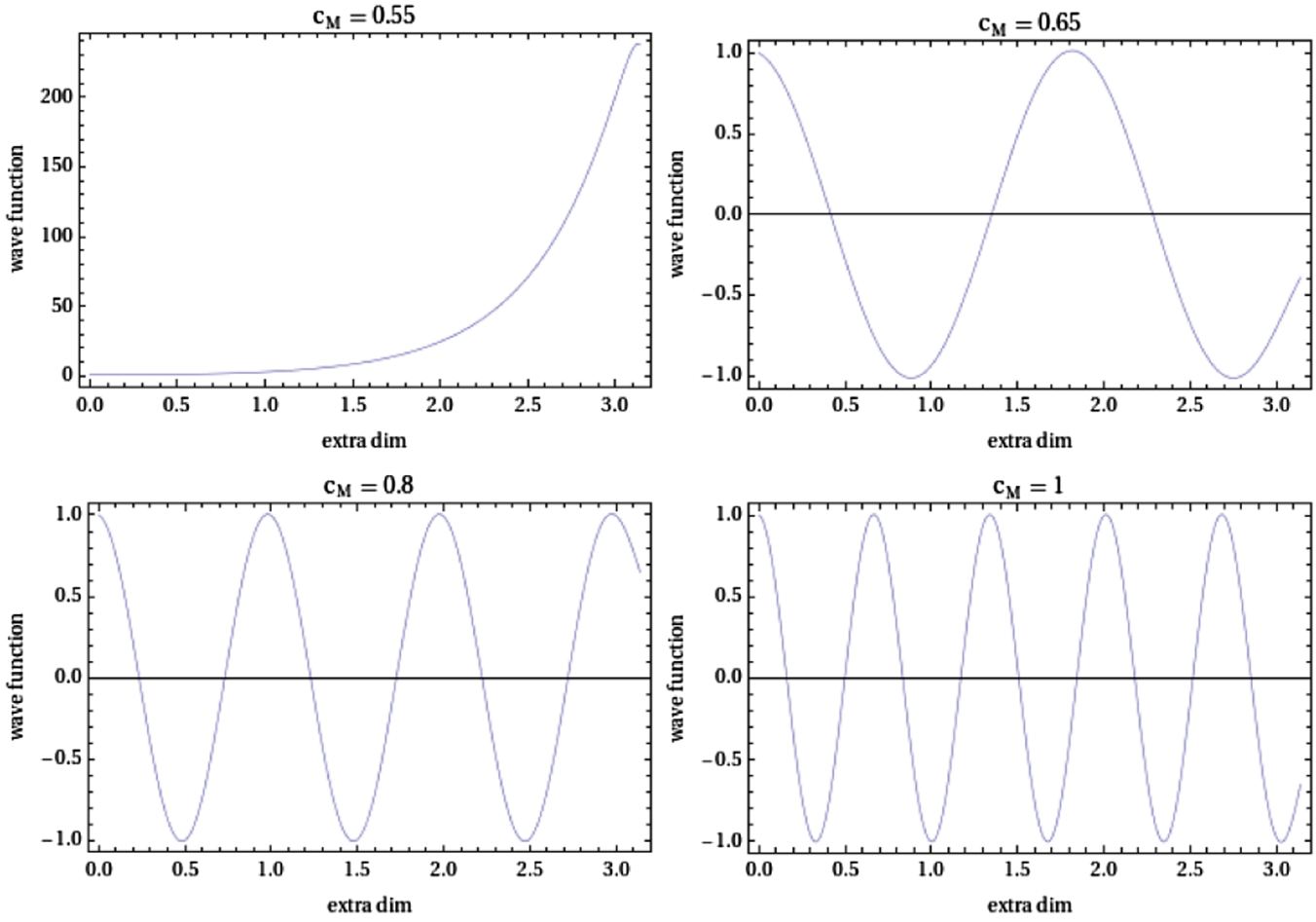

FIG. 10 (color online). The Figure shows the form of the profile for solution to Eq. (26) for a fixed bulk dirac mass of 0.58 for the right-handed neutrinos. We see that the profile becomes oscillatory as c_M becomes greater than c_N.

TABLE VI. Sample points with corresponding fits of observables for normal and inverted hierarchy schemes in bulk Majorana case with O(1) Yukawas. The masses are in GeV.

Parameter	Normal	Inverted
M_{kk}	161.4	161.4
c_{M_i}	0.55	0.55
$g_L^{(1)}(\pi R)$	3×10^{-13}	1.2×10^{-12}
c_{L_1}	0.58	0.59
c_{L_2}	0.56	0.57
c_{L_3}	0.55	0.55
c_{E_1}	0.735	0.735
c_{E_2}	0.5755	0.575
c_{E_3}	0.501	0.501
c_{N_i}	0.58	0.58
m_e	5.09×10^{-4}	5.08×10^{-4}
m_μ	0.1055	0.1055
m_τ	1.77	1.774
θ_{12}	0.58	0.58
θ_{23}	0.80	0.8
θ_{13}	0.13	0.13
Δm^2_{sol}	7.8×10^{-23}	7.8×10^{-23}
Δm^2_{atm}	2.4×10^{-21}	2.4×10^{-21}

In Table VI, we present two sample points, one for inverted hierarchy and another for normal hierarchy, which fit the neutrino masses and mixing angles as well as charged lepton masses with the accuracy we have specified in Sec. II. Both these examples[13] have $c_M < c_N$. The corresponding Yukawa coupling matrices are presented in Eqs. (32) and (33).

Yukawa parameters for inverted hierarchy

$$Y'_N = \begin{bmatrix} 2.73 & 1.81 & .108 \\ -0.83 & 0.975 & .328 \\ 0.327 & -0.679 & .182 \end{bmatrix}$$
$$Y'_E = \begin{bmatrix} 3.44 & -0.41 & .87 \\ 0.62 & 1.583 & 0.332 \\ 2.74 & 0.55 & 2.33 \end{bmatrix}. \quad (32)$$

Yukawa parameters for normal hierarchy

[13]These solutions require that the profiles of the N fields have very small values on the UV brane.

$$Y'_N = \begin{bmatrix} 2.56 & 1.69 & 1.26 \\ -0.795 & 0.927 & 3.89 \\ 0.414 & -0.859 & 2.86 \end{bmatrix}$$
$$Y'_E = \begin{bmatrix} 2.825 & -0.41 & .87 \\ 0.62 & 1.2008 & 0.332 \\ 2.74 & 0.55 & 2.31 \end{bmatrix}. \quad (33)$$

D. Brane-localized Majorana mass term

Following our discussion with a bulk Majorana mass term, there could be special cases where the Majorana mass term could be localized on either boundary. In this case, the bulk profiles for the right-handed singlets N_i remain unchanged. The eigenvalue equations are same as in Eq. (6).

1. UV-localized mass term

The case with UV-localized Majorana mass term was studied in Refs. [29,35]. The action in this case is given as

$$S_N = \int d^4x \int dy \sqrt{-g}(\delta(y)\bar{N}N^c + m_D\bar{N}N + \delta(y-\pi R)Y_N\bar{L}\tilde{H}N), \quad (34)$$

where we have expressed $m_M = \delta(y)$. Substituting the KK expansions from Eq. (17), the effective 4-dimensional neutrino mass matrix, in the basis $\chi^T = \{\nu_L^{(0)}, N_R^{(0)}, N_R^{(1)}, N_L^{(1)}\}$, takes the form

$$\mathcal{L}_m = -\frac{1}{2}\chi^T M_N \chi;$$
$$M_N = \begin{bmatrix} 0 & \mathcal{M}_\nu^{(0,0)} & \mathcal{M}_\nu^{(0,1)} & 0 \\ \mathcal{M}_\nu^{(0,0)} & M^{\rm Maj}_{\nu^{(0,0)}} & M^{\rm Maj}_{\nu^{(0,1)}} & 0 \\ \mathcal{M}_\nu^{(0,1)} & M^{\rm Maj}_{\nu^{(0,1)}} & M^{\rm Maj}_{\nu^{(1,1)}} & M_{\rm KK} \\ 0 & 0 & M_{\rm KK} & 0 \end{bmatrix}, \quad (35)$$

where $\mathcal{M}_\nu^{(0,0)}$ is defined in Eq. (19). Let $f_N^{(1)}(0)$ denote the value of the profile of the first KK mode of N at the UV brane, i.e., y = 0 and $f_N(0)$, defined in Eq. (8), is the zero-mode profile of N evaluated at y = 0. The individual elements of Eq. (35) are then defined as $\mathcal{M}_\nu^{(0,1)} = \frac{v}{\sqrt{2}}\frac{1}{\sqrt{\pi R}}f_N(\pi R)Y'_N$; $M^{\rm Maj}_{\nu^{(0,0)}} = \frac{1}{\pi R}f_N^2(0)$; $M^{\rm Maj}_{\nu^{(0,1)}} = \frac{1}{\pi R}f_N^{(1)}(0)f_N(0)$; $M^{\rm Maj}_{\nu^{(1,1)}} = \frac{1}{\pi R}f_N^{(1)}(0)f_N^{(1)}(0)$; and $M_{\rm KK}$ is the KK mass of first KK mode of N. The small neutrino masses can be fit by choosing $c_N \sim 0.32$ for which $M^{\rm Maj}_{\nu^{(0,0)}} \sim 10^{14}$ GeV. The charged leptons are fit by choosing $c_{L,E} > 0.5$. This scenario along with flavor implications has been extensively dealt with in Ref. [35].

2. Pure Majorana Case

An interesting subcase of the bulk Majorana term would be the situation where $m_D = c_N k = 0$. As we have seen from the discussion in the previous section, in such a case, the profile equations become oscillatory. The eigenvalue equations now take the form

$$\partial_y g_L^{(n)}(y) = m_n e^\sigma g_R^{(n)}(y) - m_M g_R^{(n)}(y)$$
$$-\partial_y g_R^{(n)}(y) = m_n e^\sigma g_R^{(n)}(y) - m_M g_L^{(n)}(y). \quad (36)$$

Contrary to the Dirac + Majorana case of the previous section, the above set of equations allow solutions for zero modes, $m_0 = 0$. The solutions are given as

$$g_L(y) = N\cos\left(\frac{m_n e^\sigma}{k} - m_M y\right)$$
$$g_R(y) = N\sin\left(\frac{m_n e^\sigma}{k} - m_M y\right), \quad (37)$$

where N is the normalization factor given by $N = \sqrt{\pi R k}e^{-0.5\sigma(\pi R)}$. These solutions are consistent with the boundary conditions. The neutrino mass matrix has a specific structure in this case, as there are contributions from the first KK mode, which might be important. In the basis, $\chi^T = \{\nu_L^{(0)}, N^{(0)}, N^{(1)}\}$ the mass matrix takes the form

$$\mathcal{L}_m = -\frac{1}{2}\chi^T\mathcal{M}\chi;$$
$$\mathcal{M} = \begin{pmatrix} 0 & m_D^{(0,0)} & m_D^{(0,1)} \\ m_D^{(0,0)} & 0 & 0 \\ m_D^{(0,1)} & 0 & m_{(1)} \end{pmatrix}. \quad (38)$$

From the above, we see that at the zeroth level, light neutrino and singlet neutrinos form a pseudo-Dirac structure, leading to maximal mixing between these two states. For the three flavor states, we would have three light states which are sterile. We have not pursued the phenomenology of this model further.

III. LEPTON-FLAVOR VIOLATION

We now study lepton flavor violating constraints on the three neutrino mass models considered in the present work. Lepton-flavor violation within the RS framework has been studied in detail in Ref. [30]. The localization of the fermions in the bulk at different places leads to nonzero flavor mixing between the zero-mode SM fermions and higher KK states, which contribute to flavor-violating processes both at the tree and the loop level. The tree-level flavor-violating decay modes of the form $l_i \to l_j l_k l_k$ are due to nonuniversal overlap of the zero-mode fermions with the Z-boson KK modes. At the 1-loop level, penguin graphs contribute to rare decays like $l_j \to l_i + \gamma$. The SM states mix with their heavier KK states on the IR brane, and thus may give rise to significant contributions to dipole processes, in particular. The present lepton flavor violating (LFV) limits are very strong and are listed in Table VII.

In this section, we calculate the branching fractions for the leptonic flavor-changing neutral current (FCNC). The

effective 4-dimensional Lagrangian describing $l \to l'$ process is given by [30]

$$\begin{aligned}-\mathcal{L}_{\text{eff}} &= A_R(q^2)\frac{1}{2m_\mu}\bar{e}_R\sigma^{\mu\nu}F_{\mu\nu}\mu_L \\ &+ A_L(q^2)\frac{1}{2m_\mu}\bar{e}_L\sigma^{\mu\nu}F_{\mu\nu}\mu_R \\ &+ \frac{4G_F}{\sqrt{2}}[a_3(\bar{e}_R\gamma^\mu\mu_R)(\bar{e}_R\gamma_\mu e_R) \\ &+ a_4(\bar{e}_L\gamma^\mu\mu_L)(\bar{e}_L\gamma_\mu e_L) + a_5(\bar{e}_R\gamma^\mu\mu_R)(\bar{e}_L\gamma_\mu e_L) \\ &+ a_6(\bar{e}_L\gamma^\mu\mu_L)(\bar{e}_R\gamma_\mu e_R)] + \text{H.c.} \end{aligned} \tag{39}$$

A. Tree-level decays

The breaking of the electroweak symmetry at the IR brane mixes the zero-mode gauge boson with the higher modes. To parametrize this mixing, let $(Z^{(0)}, Z^{(1)})$ and $(Z'^{(0)}Z'^{(1)})$ denote the gauge boson states before and after diagonalization of the gauge boson mass matrix, respectively. Assuming only one KK mode for simplicity, they are related as [30]

$$\begin{aligned} Z'^{(0)} &= Z^{(0)} + \sqrt{2kR\pi}\frac{m_Z^2}{M_{Z^{(1)}}^2}Z^{(1)} \\ Z'^{(1)} &= Z^{(1)} - \sqrt{2kR\pi}\frac{m_Z^2}{M_{Z^{(1)}}^2}Z^{(0)}, \end{aligned} \tag{40}$$

where $M_{Z^{(1)}}$ is the mass of first KK excitation of the Z boson. Owing to its flat profile, the $Z^{(0)}$ couples universally to all three generations. However, the coupling of $Z^{(1)}$, whose profile is peaked near the IR brane, is generation-dependent. This coupling depends on the localization of the fermions along the extra dimension, thus giving rise to nonuniversality. Let $\eta^T = \{e_M, \mu_M, \tau_M\}$ be vector of fermions in the mass basis. Let $a_{ij}^{(1)}$ be a 3×3 matrix which denotes the coupling of SM fermions in the mass basis to $Z'^{(1)}$. It is given as

TABLE VII. Present Experimental Bounds on LFV Processes

Process	Experiment	Present upper bound
BR($\mu \to e\gamma$)	MEG [49,50]	2.4×10^{-12}
BR($\mu \to eee$)	MEG [49,50]	1.0×10^{-12}
CR($\mu \to e$ in **Ti**)	SINDRUM-II [51]	6.1×10^{-13}
BR($\tau \to \mu\gamma$)	*BABAR*/Belle [52]	4.4×10^{-8}
BR($\tau \to e\gamma$)	*BABAR*/Belle [52]	3.3×10^{-8}
BR($\tau \to \mu\mu\mu$)	*BABAR*/Belle [52]	2.0×10^{-8}
BR($\tau \to eee$)	*BABAR*/Belle [52]	2.6×10^{-8}

$$a_{L,R}^{(1)ij} = g_{L,R}\bar{\eta}_{L,R}.D_{L,R}^\dagger.\begin{bmatrix} I_e & 0 & 0 \\ 0 & I_\mu & 0 \\ 0 & 0 & I_\tau \end{bmatrix}.D_{L,R}.\eta_{L,R}Z'^{(1)}, \tag{41}$$

where $g_{L,R}$ is the SM coupling, $D_{L,R}$ are 3×3 unitary matrices for rotating the zero-mode (SM) fermions from the flavor basis to the mass basis. I is the overlap of the profiles of two zero-mode fermions and the first KK gauge boson. It is given by

$$I(c) = \frac{1}{\pi R}\int_0^{\pi R} dy e^{\sigma(y)}(f_i^{(0)}(y, c))^2\xi^{(1)}(y). \tag{42}$$

$\xi^{(1)}(y)$ denotes the profile of the first KK gauge boson. It is plotted as a function of a generic bulk mass parameter c in Fig. [13]. As we can see from this figure, the overlap function $I(c)$ becomes universal for $c > 0.5$ and for $c \lesssim -15$. The of-diagonal elements of $a_{ij}^{(1)}$ represent the flavor-violating couplings. The contribution to $l_i \to l_j l_k l_k$ from direct $Z^{(1)}$ exchange is suppressed compared to that of $Z^{(0)}$. The contributions to the coefficients $a_{3,..,6}^{ij}$ in Eq. (39) due to the flavor-violating coupling of $Z^{(0)}$ as well as direct $Z^{(1)}$ exchange are given as

$$\begin{aligned} a_3^{ij} &= -2g_R(\sqrt{2kR\pi} - I_j)\frac{m_Z^2}{M_{Z^{(1)}}^2}a_R^{(1)ij} \\ a_4^{ij} &= -2g_L(\sqrt{2kR\pi} - I_j)\frac{m_Z^2}{M_{Z^{(1)}}^2}a_L^{(1)ij} \\ a_5^{ij} &= -2g_L(\sqrt{2kR\pi} - I_j)\frac{m_Z^2}{M_{Z^{(1)}}^2}a_R^{(1)ij} \\ a_6^{ij} &= -2g_R(\sqrt{2kR\pi} - I_j)\frac{m_Z^2}{M_{Z^{(1)}}^2}a_L^{(1)ij}. \end{aligned} \tag{43}$$

The branching fractions for the tree-level decays are given as [30]

$$\begin{aligned} \text{BR}(\mu \to 3e) &= 2(|a_3^{\mu e}|^2 + |a_4^{\mu e}|^2) + |a_5^{\mu e}|^2 + |a_6^{\mu e}|^2 \\ \text{BR}(\tau \to 3\mu) &= \{2(|a_3^{\tau\mu}|^2 + |a_4^{\tau\mu}|^2) + |a_5^{\tau\mu}|^2 + |a_6^{\tau\mu}|^2\} \\ &\quad \times \text{BR}(\tau \to e\nu\nu) \\ \text{BR}(\tau \to 3e) &= \{2(|a_3^{\tau e}|^2 + |a_4^{\tau e}|^2) + |a_5^{\tau e}|^2 + |a_6^{\tau e}|^2\} \\ &\quad \times \text{BR}(\tau \to e\nu\nu) \\ \text{BR}(\tau \to \mu ee) &= \{|a_3^{\tau\mu}|^2 + |a_4^{\tau\mu}|^2 + |a_5^{\tau\mu}|^2 + |a_6^{\tau\mu}|^2\} \\ &\quad \times \text{BR}(\tau \to e\nu\nu) \\ \text{BR}(\tau \to e\mu\mu) &= \{|a_3^{\tau e}|^2 + |a_4^{\tau e}|^2 + |a_5^{\tau e}|^2 + |a_6^{\tau e}|^2\} \\ &\quad \times \text{BR}(\tau \to e\nu\nu). \end{aligned} \tag{44}$$

Similarly, the relevant quantities for $\mu \to e$ conversion in Ti are given as

$$a_{L,R}^{\mu e} = -\sqrt{2kR\pi}\frac{m_Z^2}{M_{Z^{(1)}}^2}a_{L,R}^{(1)\mu e}$$

$$\mathrm{BR}(\mu \to e)\ \text{in Nuclei} = \frac{2p_e F_p^2 E_e G_F^2 m_\mu^3 \alpha^3 Z_{eff}^4 Q_N^2}{\pi^2 Z\Gamma_{\text{capt}}}[|a_R^{\mu e}|^2 + |a_L^{\mu e}|^2], \quad (45)$$

where $p_e \sim E_e \sim m_\mu$. G_F is the Fermi constant, and α is the electromagnetic coupling. The most stringent constraint for $\mu - e$ conversion comes from titanium (Ti_{22}^{48}). Atomic constants are defined as $Q_N = v^u(2Z + N) + v^d(2N + Z)$ with N being the neutron number, $Z_{\text{eff}} = 17.61$, form factor $F_p = 0.55$, $\Gamma_{\text{capt}} = 2.6 \times 10^6\ \mathrm{s}^{-1}$ for titanium [53].

B. Dipole Transition $l_j \to l_i\gamma$

The dominant graph is due to scalar exchange in the loop. One of them is due to Higgs exchange as shown in Fig. 12. The amplitude for this process is given as

$$M_{j\to i\gamma} = \sum_{n,m}\int \frac{d^4k}{(2\pi)^4}\bar{u}_i(p')\Lambda_L^{i\dagger}Y_E'\frac{\hat{p}' + M_n}{\hat{p}'^2 - M_n^2}e\gamma^\mu\frac{\hat{p} + M_n}{\hat{p}^2 - M_n^2} \times vY_E'^\dagger\frac{\hat{p} + M_m}{\hat{p}^2 - M_m^2}Y_E'\Lambda_R^j u_i(p)\frac{1}{k^2 - m_H^2}\epsilon_\mu, \quad (46)$$

where $\hat{p} = p - k$, $\hat{p}' = p' - k$ and $q = p - p'$. $\Lambda_{L,R}^i = F_{L,R}^i D_{L,R}$ and M_n denotes the mass of the nth-mode KK fermion. $F_{L,E}$ is a function of bulk masses which are taken to be diagonal in the flavor space. It is given as

$$F_{L,R} = \begin{bmatrix} f_{c_{L_1},c_{E_1}}(\pi R) & 0 & 0 \\ 0 & f_{c_{L_2},c_{E_2}}(\pi R) & 0 \\ 0 & 0 & f_{c_{L_3},c_{E_3}}(\pi R) \end{bmatrix}. \quad (47)$$

The amplitude for Eq. (46) can be rewritten as

$$M(j \to i\gamma) = (eD_L^\dagger F_L Y_E' Y_E'^\dagger vY_E' F_R D_R)_{ij} J(\hat{p}, \hat{p}', q). \quad (48)$$

The expression $J(\hat{p}, \hat{p}', q)$ is the momentum integral in Eq. (46). It is log-divergent owing to a double-independent sum over two KK modes. We regularize it using a cutoff of $\Lambda \sim 4\pi M_{kk}^{(1)} \sim 15$ TeV. The other dominant contribution is due to Fig. 19 as discussed in Appendix B. The branching fraction for the dipole decays $l_j \to l_i\gamma$ is given as

$$\mathrm{BR}(l_j \to l_i\gamma) = \frac{12\pi^2}{(G_F m_j^2)^2}(A_L^2 + A_R^2), \quad (49)$$

where the coefficient due to Figs. 12 and 19 is given as

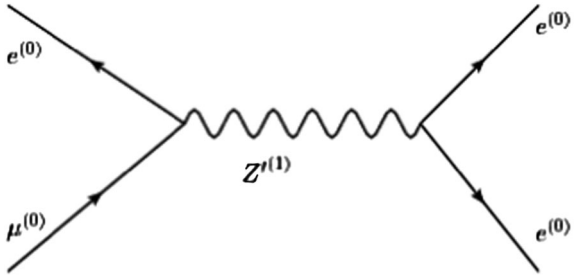

FIG. 11. Tree-level contribution to $\mu \to eee$ due to exchange of $Z'^{(1)}$. The effective $Z^{(0)}$ contribution is proportional to this graph.

$$A_L = 2\frac{em_j}{16\pi^2}\frac{1}{M_{KK}^2}\frac{v}{\sqrt{2}}D_L^\dagger F_L(Y_N'Y_N'^\dagger + Y_E'Y_E'^\dagger)Y_E F_R D_R \quad (50)$$

and $A_R = A_L^\dagger$. The other dipole contributions are discussed in Appendix B. We now proceed to discuss the LFV rates for the mass models discussed in Sec. II. The quantities, like the KK masses of fermions, the rotation matrices $D_{L,R}$, etc., which determine the LFV rates are functions of the bulk mass parameters. We compute these quantities for each point of the best-fit parameter space obtained earlier for the LH.LH and the Dirac case and use it to constrain the parameter space from flavor violation.

C. LH.LH Case

The contributions to trilepton decays from graphs like Fig. 11 are highly suppressed in the parameter space of interest. This is because the couplings of the zero-mode fermions to the KK gauge boson become universal for the fermions sufficiently localized toward IR and UV branes, as can be seen in Fig. 13. However, there could be other potentially large contributions. This comes from the large mixing between zero-mode charged singlet states and the first KK modes of the lepton doublets; the corresponding Yukawa coupling is very large due to the large negative c_E values. An example of such a graph is shown in Fig. 14. Exact value of the contribution, of course, depends on the

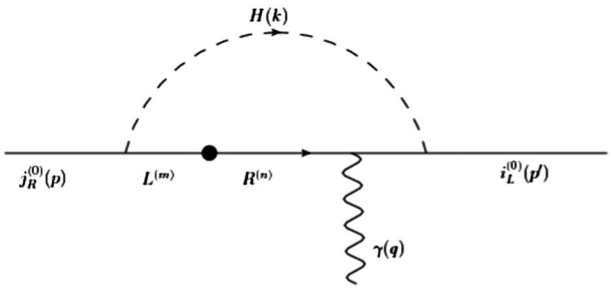

FIG. 12. Higgs-mediated $j \to i\gamma$. The dot represents the mass insertion. Flavor indices have been suppressed in the internal charged KK lines. (L, R) represents the KK modes corresponding to the left and right chiral zero modes.

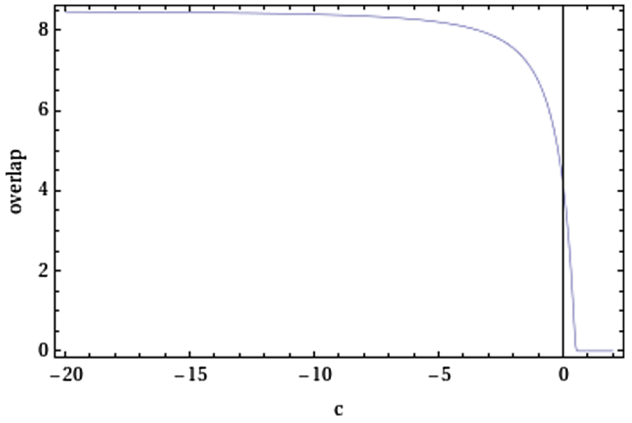

FIG. 13 (color online). Coupling of two zero-mode fermions to Z_1 as a function of bulk mass parameter [42].

values of $D_{L,R}$ and other parameters. We have not considered these graphs in the present work. We note that for a fairly degenerate bulk doublet masses, c_{L_i}, the combination of the matrices which enter in these graphs are aligned with the zero-mode mass matrix for charged leptons. The best parameter space does contain such regions where all the c_{L_i} are degenerate. We found several examples of that kind. Another potential problem with the highly localized IR charged singlets is the shift in the universal coupling constant g_R. This could effect $Z \to ll$ branching fractions. Models with custodial symmetries or very heavy KK gauge bosons could avoid this problem. We have not addressed this issue here.

Finally, contribution to $l_j \to l_i \gamma$ due to loop diagrams of the form in Fig. 20 are heavily suppressed owing to the heavy KK mass scales corresponding to the charged singlets. The corresponding masses are in shown in Table II. Additionally, the large effective 4-dimensional Yukawa couplings of the charged singlets to the KK modes make it difficult to apply techniques of perturbation theory to calculate graphs like those in Fig. 12 and 19.

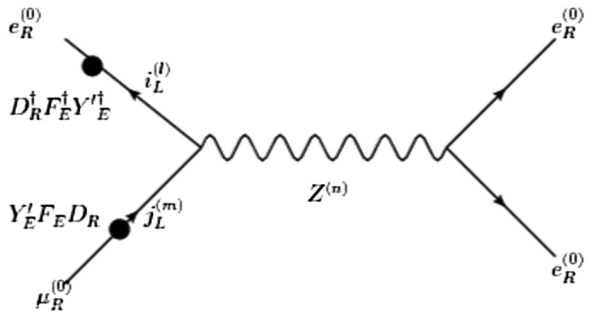

FIG. 14. Additional tree-level contribution to $\mu \to eee$. For a fairly degenerate bulk doublet mass in the LH.LH case, this contribution is negligible. For the Dirac case, this graph receives wave-function suppression in addition to the KK scale suppression.

TABLE VIII. BR for dipole decays for the case with bulk Majorana mass

Hierarchy	BR($\mu \to e\gamma$)	BR($\tau \to \mu\gamma$)	BR($\tau \to e\gamma$)
Inverted	2.4×10^{-5}	1.9×10^{-5}	7.6×10^{-6}
Normal	1.4×10^{-5}	3.4×10^{-5}	1.3×10^{-5}

D. Constraints on Dirac neutrinos

The Dirac case gives a good fit to the leptonic data for a reasonable choice of $\mathcal{O}(1)$ parameters. However, the parameter space is strongly constrained from flavor considerations. In the parameter space of interest, the dominant contribution to tree-level decays comes from Fig. 11. The parameter space of the bulk doublets and charged singlets consistent with tree-level contribution is shown in Fig. 15. The lightest $M_{Z^{(1)}}$ mass required to satisfy all constraints from tree-level processes $\sim$1.9 TeV. Fig. 15 shows the points within the best-fit parameter space consistent with all constraints from tree-level processes. As can be seen from the figure, very few points pass the constraints. The black point is allowed for a KK gauge boson scale of 1.9 TeV, whereas the green points are for mass of 3 TeV. The constraints from dipole processes are far more severe. Corresponding to the $c_{L,E}$ values in the best-fit parameter space, the mass of the first KK excitation of the leptons varied from approximately 850 GeV to 1400 GeV as presented in Table IV. We found no points which satisfied the constraints from $\mu \to e\gamma$, $\tau \to e\gamma$ and $\tau \to \mu\gamma$ simultaneously. The constraint from $\mu \to e\gamma$ was most severe and required a KK fermion mass scale $\mathcal{O}(10)$ TeV to suppress it below the experimental limit given in Table VII.

E. Constraints on scenarios with bulk Majorana mass

The tree-level decays only constrain the parameter space of the bulk doublets and charged singlets as seen in Fig. 15. Since the charged lepton mass fitting is independent of any right-handed neutrino parameter, the constraints coming from tree-level decays in the Dirac case are applicable in this case as well.

The contribution to dipole decays of the form $l_j \to l_i \gamma$ due to charged Higgs shown in Fig. 19 is small. This is because, as shown in Table VI, $g_L^{(1)}(\pi R)$ is required to be small to fit neutrino masses. Thus, the dominant contribution to dipole decays in this case is due to the Higgs exchange diagram shown in Fig. 12. These contributions are calculated for the both the normal and inverted hierarchy cases presented earlier and are given in Table VIII. The branching fractions are evaluated for $M_{KK} \sim$ 1250 GeV which is the first KK scale of the doublet.

IV. MINIMAL FLAVOR VIOLATION

From the discussion above, it is clear that lepton flavor violating constraints are strong on RS models with

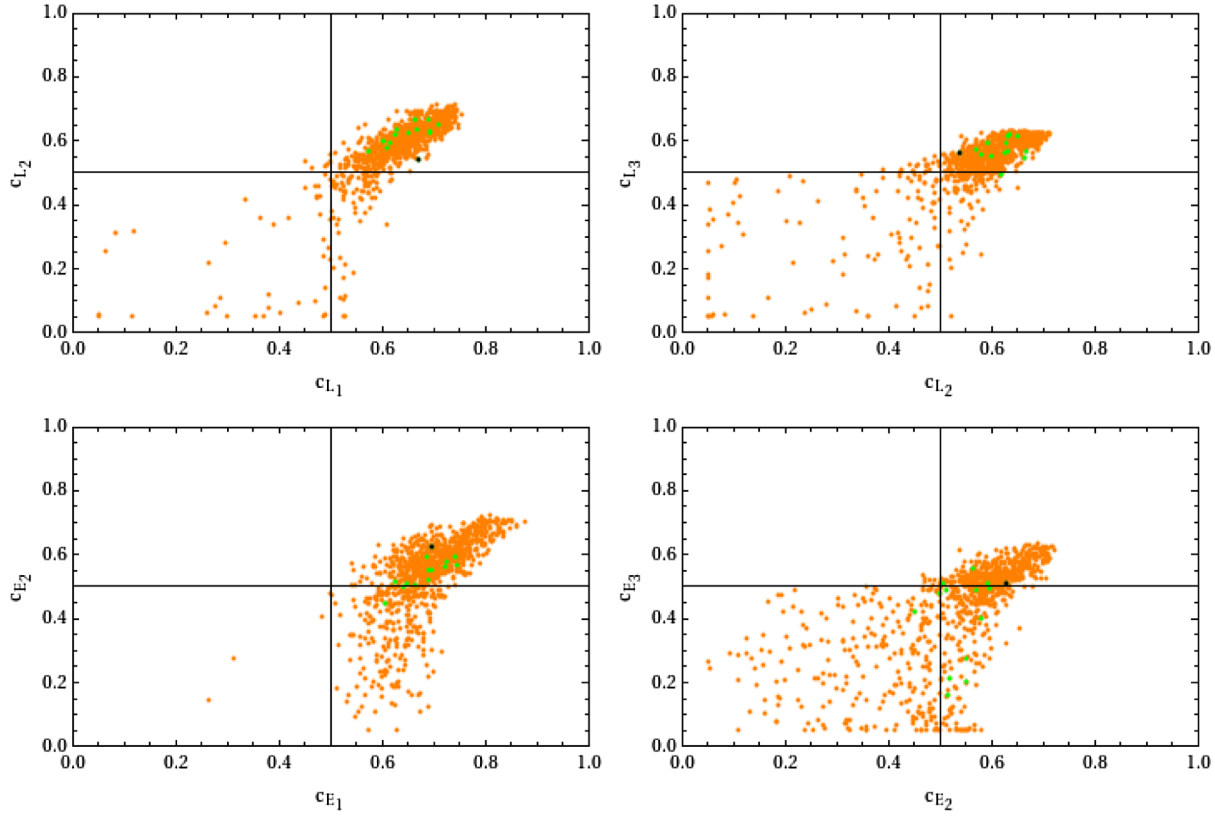

FIG. 15 (color online). The black dot and the green region represent the parameter space permitted by tree-level constraints for a KK gauge boson scale of 1920 and 3000 GeV, respectively.

fermions localized in bulk and Higgs localized on the IR brane. In the Dirac and the bulk seesaw case, flavor violation rules out most of the best-fit parameter space. One option to evade these bounds would be to increase the scale of KK masses. As we have seen previously, in the LH.LH case, the fits indicate a highly hierarchial KK spectrum for singlet charged sleptons, with the lightest KK mode at $\sim 10^2$ TeV. The flavor violating amplitudes are highly suppressed in this case, and thus there are no strong constraints on the model. However, the Dirac and the Majorana cases whose best-fit regions have a lighter KK spectrum would essentially be ruled out. The misalignment between the Yukawa coupling matrix and bulk mass terms which determine the profile is the cause of the large flavor-violating transitions leading to strong restrictions on these models. In Ref. [54], the authors imposed discrete symmetries to constrain FCNCs. In this work, we adopt the minimal-flavor-violation ansatz which reduces the misalignment by demanding an alignment between the Yukawa matrices and the bulk parameters.

The ansatz of minimal flavor violation was first proposed for the hadronic sector [55]. It proposes that new

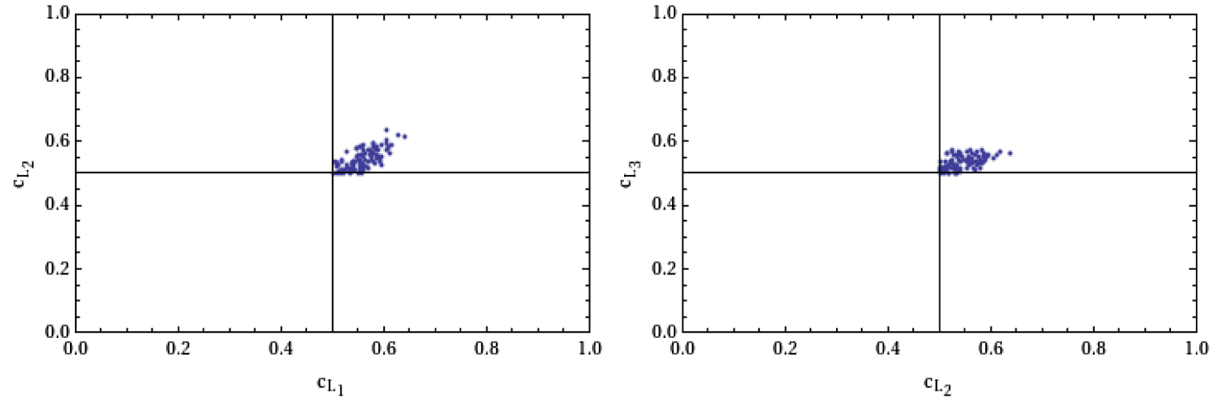

FIG. 16 (color online). The plot represents the parameter space for the bulk masses of charged doublets for inverted hierarchy.

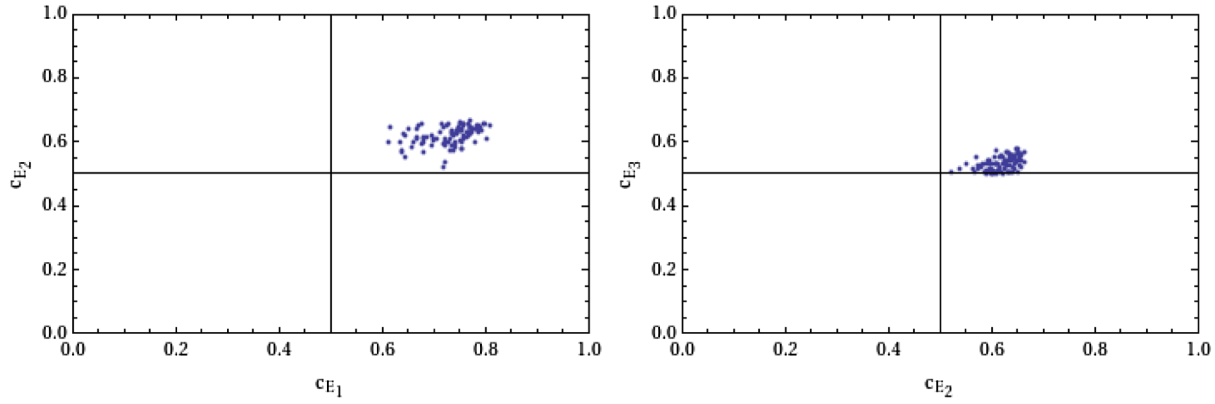

FIG. 17 (color online). The plot represents the parameter space for the bulk masses of charged singlets for inverted hierarchy.

physics adds no new flavor structures, and thus entire flavor structure in nature is determined by the Standard Model Yukawa couplings. In the leptonic sector, MFV in not uniquely defined due to the possibility of the seesaw mechanism. Several schemes of leptonic minimal flavor violation are possible [56].

The proposal to use the MFV hypothesis in RS was first introduced in Ref. [31] in the quark sector. There were subsequent extensions in the leptonic sector by Refs. [32,35]. The MFV ansatz assumes that the Yukawa couplings are the only sources of flavor violation. In the RS setting, this would require that the bulk mass terms should now be expressed in terms of the Yukawa couplings [31]. The exact expression would depend on the particle content and the flavor symmetry assumed.

A. Dirac Neutrino Case

In the presence of right-handed neutrinos, the flavor group is $SU(3)_L \times SU(3)_E \times SU(3)_N$; the lepton number is conserved. The Y_E transforms as $Y_E \rightarrow (3, \bar{3}, 1)$, and Y_N transforms as $Y_N \rightarrow (3, 1, \bar{3})$. The Yukawa couplings are aligned with the 5-dimensional bulk mass matrices. The bulk masses can be expressed in terms of the Yukawas as

$$c_L = a_1 I + a_2 Y'_E Y'^{\dagger}_E + a_3 Y'_N Y'^{\dagger}_N \qquad c_E = b Y'^{\dagger}_E Y'_E$$
$$c_N = c Y'^{\dagger}_N Y'_N, \tag{51}$$

where a, b, $c \in \Re$ and $Y'_{E,N}$ are as defined earlier as $Y'_{E,N} = 2kY_{E,N}$. Owing to the flavor symmetry, we work in a basis in which Y'_E is diagonal. We then rotate Y'_N by the neutrino mixing matrix, Pontecorvo-Maki-Nakagawa-Sakata (PMNS) matrix, i.e., writing $Y'_N \rightarrow V_{\mathrm{PMNS}} \mathrm{Diag}(Y'_N)$ where the $\mathrm{Diag}(Y'_N) = \mathrm{Diag}(0.709, 0.709, 0.75)$. The c_L value chosen is 0.5802 for all three generations. The c_N values chosen are, respectively, 1.17241, 1.172, and 1.311. The bulk singlet mass parameters are $c_E = (0.7477, 0.58059, 0.401)$.

The simplest Yukawa combination transforming as (8, 1, 1) under the flavor group is given as

$$\Delta = Y'_N Y'^{\dagger}_N. \tag{52}$$

Thus, the branching ratio (BR) for $\mu \rightarrow e\gamma$, which is the most constrained, is given as [35]

$$\mathrm{BR}(\mu \rightarrow e\gamma) = 4 \times 10^{-8} (Y'_N Y'^{\dagger}_N)^2_{12} \left(\frac{3\ \mathrm{TeV}}{M_{\mathrm{KK}}}\right)^4, \tag{53}$$

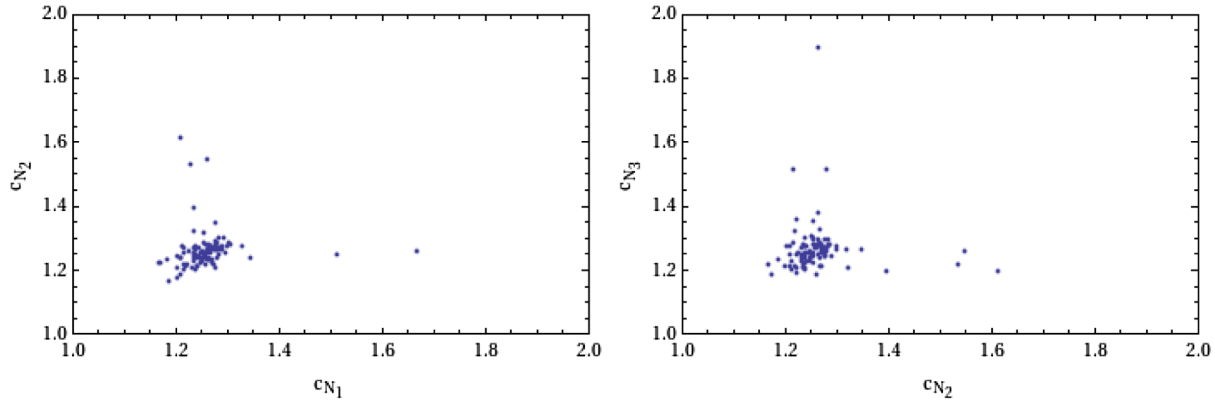

FIG. 18 (color online). The plot represents the parameter space for the bulk masses of neutrino singlets for inverted hierarchy.

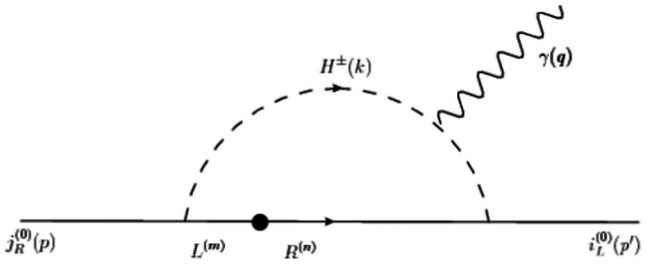

FIG. 19. "Charged" Higgs mediated $j \to i\gamma$. The dot represents the mass insertion. Flavor indices have been suppressed in the internal neutral KK lines. (L,R) represents the KK modes corresponding to the left and right chiral zero modes, respectively.

$$Y'_N = \begin{bmatrix} 0.586033 & 0.383951 & 0.115044 \\ -0.335962 & 0.370429 & 0.53165 \\ 0.215349 & -0.466953 & 0.516346 \end{bmatrix}. \quad (54)$$

The (1, 2) element of Δ which is responsible for $\mu \to e\gamma$ is 0.006 which gives a contribution of 1.44×10^{-12} for a fermion KK mass of around 3 TeV.

B. Bulk Majorana mass term

Owing to the presence of a bulk Majorana mass term, we choose the flavor group for the Lagrangian in Eq. (22) as $SU(3)_L \times SU(3)_E \times O(3)_N$. Y_E transforms as $Y_E \to (3, \bar{3}, 1)$, and Y_N transforms as $Y_N \to (3, 1, 3)$. The bulk Majorana term $\bar{N}^c N$ transforms as (1, 1, 6) under this flavor group. In terms of the dimensionless Yukawa couplings, $Y'_{E,N}$ the bulk mass parameters can be expressed as

$$c_L = a_1 I + a_2 Y'_E Y'^{\dagger}_E + a_3 Y'_N Y'^{T}_N \qquad c_E = 1 + b Y'^{\dagger}_E Y'_E$$
$$c_N = 1 + c Y'^{T}_N Y'_N \qquad c_M = d I_{3\times 3}, \quad (55)$$

TABLE IX. Sample points for inverted hierarchy in LH.LH case with O(1) Yukawas. The masses are in GeV.

Point	A	B
χ^2	7.48	6.61
c_{L_1}	0.8967	0.9162
c_{L_2}	0.8983	0.8920
c_{L_3}	0.8913	0.8945
c_{E_1}	−3758.1502	−2099.8993
c_{E_2}	−6005847.4955	−552577.8188
c_{E_3}	−32730342.0982	−23953472.2265
m_e	5.11×10^{-4}	5.09×10^{-4}
m_μ	0.1056	0.1056
m_τ	1.775	1.755
θ_{12}	0.584	0.55
θ_{23}	0.829	0.875
θ_{13}	0.148	0.160
δm^2_{sol}	7.49×10^{-23}	7.46×10^{-23}
δm^2_{atm}	1.90×10^{-21}	2.7×10^{-21}

where $a, b, c, d \in \Re$. $c_M = 0.55$ and $c_N = 0.58$ are chosen for the right-handed neutrino bulk mass parameters. The value of profiles for the singlets are chosen appropriately at the boundary so as to fit the neutrino data using the $\mathcal{O}(1)$ Yukawa couplings. As before, we work in a basis in which Y'_E is diagonal. In this basis, $Y'_N = V_{\text{PMNS}}\text{Diag}(Y'_N)$. This removes the dominant contribution to dipole decays due to the Higgs exchange in Fig. 12. The contribution due to Fig. 19 is very small owing to wave-function suppression of the singlet neutrinos. Thus, we see that the MFV ansatz is successful in suppressing FCNCs for both the Dirac and the bulk Majorana case.

V. SUMMARY AND OUTLOOK

Understanding neutrino masses and mixing is an important aspect of most physics beyond the Standard Model frameworks. The Randall-Sundrum setup, while solving the hierarchy problem, could also form a natural setting to explain flavor structure of the Standard Model Yukawa couplings. The quark sector has already been explored in this context in detail. While there have been several analyses in the leptonic sector, in the present work, we have tried to explore the same in a comprehensive manner, filling the gaps wherever we found it necessary. Our aim had been to determine quantitavely the parameter space of both the $\mathcal{O}(1)$ (dimensionless) Yukawa couplings as well as the bulk mass parameters which can give good fits to the leptonic data.

We have concentrated on the RS setup with the Higgs field localized on the IR boundary. We have considered three cases of neutrino mass models: (a) the LH.LH higher-dimensional operator, (b) the Dirac case, and (c) the Majorana case. The LH.LH fits require large negative c parameters which reflect the composite nature of the charged singlets. There is some parameter space in this case where the flavor constraints are weak. However, the model has very large effective 4-dimensional Yukawa couplings between the zero-mode SM fermions and the KK fermions, which makes it unattractive from a perturbation theory point of view. We have also presented the distributions of the Yukawa couplings in the best-fit region. Most of the individual Yukawa couplings are concentrated on the higher side of the $\mathcal{O}(1)$ range we have chosen. The Dirac and Majorana cases offer large parameter space without the need of large hierarchies in the c parameters. We have also presented the distribution of the Yukawa couplings in the Dirac case. We could not find strong correlations between the Yukawa couplings and the c parameters. There are strong constraints from the lepton flavor violating rare processes. These can be circumvented by a suitable choice of Yukawa couplings and c parameters guided by the MFV ansatz. The Majorana case, in particular, allows for several classes of MFV schemes, which will be explored in an upcoming publication [57].

TABLE X. Sample points for inverted hierarchy in Dirac case with O(1) Yukawas. The masses are in GeV.

Parameter	Point A	Point B
χ^2	0.30	8.04
c_{L_1}	0.5565	0.51
c_{L_2}	0.5556	0.5316
c_{L_3}	0.5433	0.5012
c_{E_1}	0.7681	0.8092
c_{E_2}	0.6186	0.6498
c_{E_3}	0.5044	0.5674
c_{N_1}	1.2450	1.2765
c_{N_2}	1.2421	1.2755
c_{N_3}	1.2546	1.2941
m_e	5.1×10^{-4}	5.08×10^{-4}
m_μ	0.1055	0.1055
m_τ	1.769	1.81
θ_{12}	0.59	0.59
θ_{23}	0.80	0.72
θ_{13}	0.155	0.152
δm^2_{sol}	7.49×10^{-23}	7.48×10^{-23}
δm^2_{atm}	2.40×10^{-21}	2.16×10^{-21}

While we restricted ourselves to the Higgs located on the IR brane; it can also be allowed to propagate in the bulk. Lepton flavor violating amplitudes, however, are now cutof-independent, which makes the computations more predictive. But with the Higgs boson in the bulk, one has to invoke other scenarios like supersymmetry to solve the hierarchy problem.

ACKNOWLEDGMENTS

We thank Bhavik Kodrani for important and interesting input. We appreciate D. Chowdhury and R. Garani's help with the numerics. We also thank V. S. Mummidi for carefully reading the manuscript. S. K. V. acknowledges support from DST Ramanujam Fellowship SR/S2/RJN-25/2008 of Government of India.

APPENDIX A: INVERTED MASS FITS

We present the results of the scan performed for inverted hierarchy for both the LH.LH and the Dirac case. In the case for the normal hierarchy, it was easier to find c values and order-one Yukawa entries which satisfied all constraints. However, the choice of these parameters which fit the data in the inverted case is very subtle. This is because one requires two large mass eigenvalues in the inverted case which must satisfy the Δm^2_{sol} constraint. This requires a very careful choice of order-one Yukawa parameters. The parameter space for c values does not differ much between the normal and the inverted case. For the case of inverted hierarchy, we choose points which satisfy $0 < \chi^2 < 10$. Sample points for the LH.LH case that fit the data are given in Table IX, and the corresponding Yukawa couplings are given in Eqs. (A1) and (A2). For the Dirac case, we performed a scan only for $c > 0.5$. The results are summarized in a similar fashion to the hierarchial case, in Figs. 16–18, where the allowed parameter space in the bulk parameters is shown. Two sample points that fit the data are shown in Table X. The corresponding Yukawa couplings are given in Eqs. (A3) and (A4).

1. LHLH case

Yukawa for Point A

$$Y'_E = \begin{bmatrix} 0.8249 & 0.8516 & 1.1111 \\ 1.3600 & 1.5956 & 1.8402 \\ 3.5831 & 3.5664 & 2.9092 \end{bmatrix};$$
$$\kappa' = \begin{bmatrix} -3.5528 & 2.6612 & 1.4503 \\ 2.6612 & 3.8149 & 1.2903 \\ 1.4503 & 1.2903 & -0.6682 \end{bmatrix}. \quad \text{(A1)}$$

Yukawa for Point B

$$Y'_E = \begin{bmatrix} 2.5874 & 0.5123 & 3.6064 \\ 3.9696 & 2.4876 & 1.9903 \\ 3.8604 & 1.1438 & 3.9712 \end{bmatrix};$$
$$\kappa' = \begin{bmatrix} -3.6860 & -3.6778 & 3.9987 \\ -3.6778 & 2.1362 & 3.3252 \\ 3.9987 & 3.3252 & -0.8497 \end{bmatrix}. \quad \text{(A2)}$$

2. Dirac Case

Yukawa for Point A

$$Y'_E = \begin{bmatrix} 2.2645 & 2.7691 & 0.4272 \\ 1.0499 & -3.6695 & -1.0818 \\ -2.2402 & -0.5400 & -1.9176 \end{bmatrix};$$
$$Y'_N = \begin{bmatrix} -0.2202 & -2.3054 & 1.5602 \\ 3.4794 & -2.2140 & 0.2302 \\ -2.0676 & -1.7529 & 0.7888 \end{bmatrix}. \quad \text{(A3)}$$

Yukawa for Point B

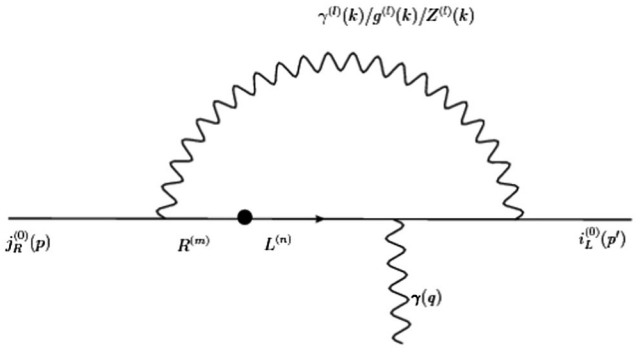

FIG. 20. Contribution to the dipole graph due exchange of KK gauge bosons and charged KK fermion lines.

$$Y'_E = \begin{bmatrix} -3.7916 & -0.3960 & -2.5573 \\ 1.2699 & -2.3757 & 3.2167 \\ -3.5010 & 3.4430 & 2.8224 \end{bmatrix}; \qquad Y'_N = \begin{bmatrix} -3.9443 & -0.9714 & 0.1848 \\ -2.5788 & 0.2609 & 3.3684 \\ 0.5020 & -3.0268 & -3.1765 \end{bmatrix}. \tag{A4}$$

APPENDIX B: AMPLITUDES FOR DIPOLE TRANSITIONS

In this section, we review the other potential contributions to the dipole processes $i \to j\gamma$.

1. Internal flip in neutrino KK line in Dirac case

This contribution (see Fig. 19) is absent for the LH.LH case as it involves neutral internal KK lines corresponding to the right-handed neutrino. In the unitary gauge, the charged Higgs is nothing but the longitudinal component of the W boson. This displays a similar divergence to Fig. 12, owing to the presence of the double KK sum.

$$M_{j\to i\gamma} = \left(F_L Y'_N Y'^{\dagger}_N e \frac{v}{\sqrt{2}} Y'_E F_E\right)_{ij} \int \sum_{n,m} \frac{d^4k}{(2\pi)^4} \bar{u}_i(p')(2k^\mu - q^\mu) \frac{(\hat{p}' + M_n)}{(\hat{p}'^2 - M_N^2)} \frac{\hat{p} + M_n}{\hat{p}^2 - M_m^2} \frac{1}{k^2 - m_H^2} \frac{1}{(k-q)^2 - m_H^2} u_j(p). \tag{B1}$$

2. Gauge contribution

Additional contributions arise due to KK gauge bosons in the loop as shown in Fig. 20.
The amplitude for Fig. 20 is given as

$$M_{j\to i\gamma} = \left(A^{0,n,l} \frac{v}{\sqrt{2}} Y'_E A^{0,m,l}\right)_{ij} \sum_{n,m} \int \frac{d^4k}{(2\pi)^4} \bar{u}_i(p') \frac{\hat{p}' + M_n}{\hat{p}'^2 - M_n^2} e\gamma^\mu \frac{\hat{p} + M_n}{\hat{p}^2 - M_n^2} \frac{\hat{p}' + M_m}{\hat{p}'^2 - M_m^2} u_j(p) \frac{1}{k^2 - m_H^2}, \tag{B2}$$

where $A^{0,n,l}$ represents the coupling of the zero-mode fermion to nth-mode fermion and lth-mode gauge boson. The contribution from this sector is suppressed in both the Dirac and LH.LH case in the parameter space under consideration.

[1] L. Randall and R. Sundrum, Phys. Rev. Lett. **83**, 3370 (1999).
[2] T. Gherghetta, arXiv:1008.2570.
[3] H. Davoudiasl, S. Gopalakrishna, E. Ponton, and J. Santiago, New J. Phys. **12**, 075011 (2010).
[4] K. Agashe, A. Delgado, and R. Sundrum, Ann. Phys. (Leipzig) **304**, 145 (2003).
[5] H. Davoudiasl, J. Hewett, and T. Rizzo, Phys. Lett. B **473**, 43 (2000).
[6] S. Chang, J. Hisano, H. Nakano, N. Okada, and M. Yamaguchi, Phys. Rev. D **62**, 084025 (2000).
[7] S. J. Huber and Q. Shafi, Phys. Rev. D **63**, 045010 (2001).
[8] C. Csaki, J. Erlich, and J. Terning, Phys. Rev. D **66**, 064021 (2002).
[9] G. Burdman, Phys. Rev. D **66**, 076003 (2002).
[10] H. Davoudiasl, J. Hewett, and T. Rizzo, Phys. Rev. D **68**, 045002 (2003).
[11] M. S. Carena, T. M. Tait, and C. Wagner, Acta Phys. Pol. B **33**, 2355 (2002).
[12] S. J. Huber, C.-A. Lee, and Q. Shafi, Phys. Lett. B **531**, 112 (2002).
[13] K. Agashe, A. Delgado, M. J. May, and R. Sundrum, J. High Energy Phys. 08 (2003) 050.
[14] J. Hewett, F. Petriello, and T. Rizzo, J. High Energy Phys. 09 (2002) 030.
[15] A. Falkowski and M. Perez-Victoria, J. High Energy Phys. 12 (2008) 107.
[16] J. A. Cabrer, G. von Gersdorff, and M. Quiros, Phys. Lett. B **697**, 208 (2011).
[17] N. Arkani-Hamed and M. Schmaltz, Phys. Rev. D **61**, 033005 (2000).
[18] C. Froggatt and H. B. Nielsen, Nucl. Phys. **B147**, 277 (1979).
[19] K. Babu, arXiv:0910.2948.
[20] K. Agashe, G. Perez, and A. Soni, Phys. Rev. D **71**, 016002 (2005).
[21] S. J. Huber and Q. Shafi, Phys. Lett. B **498**, 256 (2001).
[22] C. Delaunay, O. Gedalia, S. J. Lee, G. Perez, and E. Ponton, Phys. Rev. D **83**, 115003 (2011).
[23] S. Casagrande, F. Goertz, U. Haisch, M. Neubert, and T. Pfoh, J. High Energy Phys. 10 (2008) 094.
[24] M. Bauer, S. Casagrande, U. Haisch, and M. Neubert, J. High Energy Phys. 09 (2010) 017.
[25] Y. Grossman and M. Neubert, Phys. Lett. B **474**, 361 (2000).
[26] R. Kitano, Phys. Lett. B **481**, 39 (2000).
[27] S. J. Huber and Q. Shafi, Phys. Lett. B **512**, 365 (2001).
[28] S. J. Huber and Q. Shafi, Phys. Lett. B **544**, 295 (2002).
[29] S. J. Huber and Q. Shafi, Phys. Lett. B **583**, 293 (2004).
[30] K. Agashe, A. E. Blechman, and F. Petriello, Phys. Rev. D **74**, 053011 (2006).
[31] A. L. Fitzpatrick, L. Randall, and G. Perez, Phys. Rev. Lett. **100**, 171604 (2008).

[32] M.-C. Chen and H.-B. Yu, Phys. Lett. B **672**, 253 (2009).
[33] K. Agashe, T. Okui, and R. Sundrum, Phys. Rev. Lett. **102**, 101801 (2009).
[34] P. R. Archer, arXiv:1204.4730.
[35] G. Perez and L. Randall, J. High Energy Phys. 01 (2009) 077.
[36] C. Amsler *et al.*, Phys. Lett. B **667**, 1 (2008).
[37] M. Tortola, J. Valle, and D. Vanegas, arXiv:1205.4018.
[38] A. S. Joshipura and K. M. Patel, Phys. Rev. D **82**, 031701 (2010).
[39] C. S. Aulakh and S. K. Garg, Nucl. Phys. **B757**, 47 (2006).
[40] F. James and M. Roos, Comput. Phys. Commun. **10**, 343 (1975).
[41] T. Gherghetta, Phys. Rev. Lett. **92**, 161601 (2004).
[42] T. Gherghetta and A. Pomarol, Nucl. Phys. **B586**, 141 (2000).
[43] N. Arkani-Hamed, M. Porrati, and L. Randall, J. High Energy Phys. 08 (2001) 017.
[44] B. Batell and T. Gherghetta, Phys. Rev. D **76**, 045017 (2007).
[45] R. Contino and A. Pomarol, J. High Energy Phys. 11 (2004) 058.
[46] B. Batell and T. Gherghetta, Phys. Rev. D **77**, 045002 (2008).
[47] W. D. Goldberger, Y. Nomura, and D. Tucker-Smith, Phys. Rev. D **67**, 075021 (2003).
[48] Y. Nomura, J. High Energy Phys. 11 (2003) 050.
[49] J. Adam *et al.*, Phys. Rev. Lett. **107**, 171801 (2011).
[50] M. De Gerone and MEG Collaboration), ''μtoeγ and μtoeee Status and perspectives,'' 2011.
[51] P. Wintz *et al.* (SINDRUM II Collaboration), *Proceedings of the 14th International Conference on Particles and Nuclei (PANIC), Williamsburg, VA, 1996*, edited by C. E. Carlson and J. J. Domingo (World Scientific, Singapore, 1996), pp. 458–459.
[52] B. Aubert *et al.*, Phys. Rev. Lett. **104**, 021802 (2010).
[53] W.-F. Chang and J. N. Ng, Phys. Rev. D **71**, 053003 (2005).
[54] C. Csaki, C. Delaunay, C. Grojean, and Y. Grossman, J. High Energy Phys. 10 (2008) 055.
[55] G. D'Ambrosio, G. Giudice, G. Isidori, and A. Strumia, Nucl. Phys. **B645**, 155 (2002).
[56] V. Cirigliano, B. Grinstein, G. Isidori, and M. B. Wise, Nucl. Phys. **B728**, 121 (2005).
[57] A. M. Iyer and S. K. Vempati (work in progress).